Noname manuscript No.
(will be inserted by the editor)

Rafael de la Llave · Arturo Olvera · Nikola P. Petrov

Combination laws for scaling exponents and relation to the geometry of renormalization operators

The principle of approximate combination of scaling exponents

Received: date / Accepted: date

Abstract Renormalization group has become a standard tool for describing universal properties of different routes to chaos – period-doubling in unimodal maps, quasiperiodic transitions in circle maps, dynamics on the boundaries of Siegel disks, destruction of invariant circles of area-preserving twist maps, and others. The universal scaling exponents for each route are related to the properties of the corresponding renormalization operators.

We propose a *Principle of Approximate Combination of Scaling Exponents* (PACSE) that organizes the scaling exponents for different transitions to chaos. Roughly speaking, if the combinatorics of a transition is a composition of two simpler combinatorics, then the scaling exponents of the combined combinatorics is approximately equal to the product of the scaling exponents, both in the parameter space and in the configuration space, corresponding to each of these two combinatorics. We state PACSE quantitatively as precise asymptotics of the scaling exponents for combined combinatorics, and give convincing numerical evidence for it for each of the four dynamical systems mentioned above.

We propose an explanation of PACSE in terms of the dynamical properties of the renormalization operators – in particular, as a consequence of certain transversal intersections of the stable and unstable manifolds of the operators corresponding to different transition to chaos.

Keywords Universality · Renormalization · Scaling exponents · Combined combinatorics · Bifurcation

1 Introduction

One important discovery from the 1970's is that several bifurcation diagrams present universal scaling exponents. In the words of [9, p. 40], "the whole bifurcation diagram is crisscrossed by an infinity of asymptotically universal ratios". These scaling relations can happen among parameter values or among spatial features of the diagram. The word "universal" means that if we change the family of maps without altering its "essential features", we will obtain bifurcation diagrams that exhibit the same bifurcations and the same scaling exponents.

The research of RL has been partially supported by NSF grant DMS 0901389, and Texas Coordinating Board ARP 0223. The research of NPP has been partially supported by NSF grant DMS 0807658. RL and NPP were also supported by Big XII fellowships. The computations were carried out on the computers of the Department of Mathematics of the University of Texas and the computers of IIMAS-UNAM.

Rafael de la Llave
Department of Mathematics, University of Texas, 1 University Station C1200, Austin, TX 78712, USA
E-mail: llave@math.utexas.edu

Arturo Olvera
IIMAS-UNAM, FENOMEC, Apdo. Postal 20–726, México D.F., Mexico
E-mail: aoc@mym.iimas.unam.mx

Nikola P. Petrov (corresponding author)
Department of Mathematics, University of Oklahoma, 601 Elm Avenue, Norman, OK 73019, USA
Phone: +1-405-325-4316, fax: +1-405-325-7484
E-mail: npetrov@math.ou.edu

Quite remarkably, the existence of these scaling relations happens in very different scenarios, the most widely know ones being:

- unimodal maps [18,19,62,15];
- higher dimensional maps with disipation [11,13];
- period doubling in area-preserving maps of the plane [10,16];
- maps of the circle with critical points [51,20,50];
- boundaries of Siegel disks in the complex plane [42,64];
- invariant circles in conservative maps in two dimensions [52,40];
- non-twist (a.k.a. shearless) invariant tori in area-preserving maps [6,2,23].

Many of these exponents were related to properties of fixed points of renormalization group operators.

The goal of this paper is to investigate some order among the many exponents that have been computed or studied rigorously. More precisely, we formulate a new principle that we call the *Principle of Approximate Combination of Scaling Exponents*, or PACSE for short, and present convincing numerical evidence for it in several contexts. By the word "principle" we mean some regularity that can be expected to happen and, therefore, can be used as guidance in numerical explorations. Of course, the validity of this principle can be rigorously deduced from some other hypotheses that can in turn be established.

Roughly speaking, PACSE asserts that good approximations to some scaling exponents can be obtained by taking products of other exponents. The mathematically precise formulation of what is meant by an approximate relation is somewhat subtle – it has to involve some limit in which it becomes exact and, if possible, the rate at which this limit is approached. PACSE is concerned not only with the existence of the limit, but also with the rate of convergence. To study PACSE, we have followed two approaches – an experimental one and a mathematically rigorous one. The experimental approach – developed in this paper – consists of performing highly accurate numerical computations of many exponents in different cases. Because of the variety of phenomena studied and the need for high precision, the computations are quite challenging.

In a companion paper [35], we present some rigorous results that establish PACSE as a consequence of global properties of renormalization group operators. The mathematical result in [35] is a variation on the theme that heteroclinic cycles generate complicated behaviour. This is, of course, very well known in finite dimensions, but in our case the operators we need to consider act in infinite-dimensional spaces, and there are some complications due to the fact that the operators are not invertible (they are compact). We also need to obtain quantitative staments on the geometry of the orbits generated by the homoclinic connections. We hope that these results could also be useful in other contexts (e.g., parabolic PDEs), where similar problems appear.

We think that it is worthwhile to test the numerical methodology in places where there is a firm mathematical basis, so that it can be used to suggest new mathematical discoveries. Of course, one can also argue that taking some mathematical results into concrete high precision calculations is an enhancement as well.

We also note that the numerical verification of PACSE is an indication that the global properties of the renormalization operators hold [35], and this can serve as a motivation to undertake a more delicate study either by analytical methods or by a computer assisted proof (a similar study was undertaken in [17]).

PACSE is perhaps somewhat related to the possibility mentioned by Wilson in the final words of his famous paper on renormalization group and critical phenomena [65] that "the solutions of the renormalization group equations might approach a limit cycle or go off to infinity or go into irregular oscillations (ergodic or turbulent?)".

We note that observations of particular cases of PACSE have occurred in the literature. In the context of unimodal maps, this was noticed by Derrida *et al* in their seminal papers [14,15]. Cvitanovic *et al* [12] published some scaling exponents for critical circle maps with eventually periodic rotation numbers and discussed some universality properties. A more systematic study for unimodal maps appeared in [8], who also offered an explanation in terms of "periodic approximations". In the case of twist maps, it was observed in a paragraph in the Ph.D. thesis of one of the authors [46, Section IV.5.4, page 82]. Ge *et al* [26] and Ketoja and Kulkijärvi [32] observed some scalings of the widths of the windows in the bifurcation diagram of unimodal maps with different kneading sequences.

We have published a preliminary announcement of our results in [36].

2 Formulation of PACSE

2.1 Generalities

In the subsequent sections, we will give more details on the formulation of PACSE for each of the particular renormalization scenarios that we study, but it will be useful to start with a general overview. The precise meaning of the structures defined here will become clearer in the particular cases considered later, and we hope they will be easily recognizable to those familiar with one of the standard renormalization scenarios.

In each renormalization scenario, one selects a one-parameter familiy of maps in a certain class (e.g., unimodal maps of the interval with some non-degeneracy properties). Once we fix a family f_μ in this class, we look for a sequence of parameter values μ_n for which the map has orbits of increasingly complex combinatorial descriptions K_1, K_2, K_3, ...; we will refer to the K_j's shortly as *combinatorics*. In the unimodal map case, K_n are the kneading sequences and μ_n are the parameter values for which the map has a superstable periodic orbit with kneading sequence K_n. Let $\mathscr{K}$ stand for the set of all allowed combinatorics. We consider a sequence of combinatorics K_j that is obtained by some combinatorial construction:

$$\mathsf{K}_{j+1} = \mathscr{C}_\mathsf{A}(\mathsf{K}_j) \ .$$

The operation $\mathscr{C}_\mathsf{A} : \mathscr{K} \to \mathscr{K}$ that increases the complexity has an extra combinatorial parameter A which belongs to some set $\mathscr{K}_0 \subseteq \mathscr{K}$ that will be specified in each cases we consider.

Let μ_j be the value for which the map f_{μ_j} has orbits of combinatorics K_j. It is often found that the parameters μ_j thus obtained satisfy some scaling relations of the form

$$\mu_j \approx \mu_\infty + a\,\delta_\mathsf{A}^{-j} \ , \tag{1}$$

where δ_A it is independent of the family f_μ within a certain class of maps – hence it is said to be *universal*. The other two numbers, μ_∞ and a, generally depend on the family. The precise meaning of (1) is usually taken to be

$$\frac{\mu_{j+1} - \mu_j}{\mu_j - \mu_{j-1}} \to \delta_\mathsf{A}^{-1} \quad \text{as} \quad j \to \infty \ , \tag{2}$$

where the limit is approached exponentially fast. The number δ_A is called the *parameter-space scaling exponent*; the subscript A means that δ_A depends on the combinatorial parameter A.

It is observed at the same time that the orbits of f_{μ_j} have some spatial characteristic ℓ_j that satisfies $\ell_j \approx b\,\alpha_\mathsf{A}^{-j}$, which stands for

$$\frac{\ell_{j+1}}{\ell_j} \to \alpha_\mathsf{A}^{-1} \quad \text{as} \quad j \to \infty \tag{3}$$

for some universal α_A and family-dependent b. We refer to α_A as the *spatial* (or *configugation-space*) *scaling exponent*; again, α_A depends on A.

A crucial ingredient in the formulation of PACSE is that there is an operation $\star$ such that

$$\mathscr{C}_\mathsf{A} \circ \mathscr{C}_\mathsf{B} = \mathscr{C}_{\mathsf{A}\star\mathsf{B}} \ . \tag{4}$$

Since composition is associative – but in general not commutative – so will be the $\star$ operation.

The renormalization operator $\mathcal{R}_\mathsf{A}$ is defined for maps f with combinatorics $\mathsf{K}(f) = \mathscr{C}_\mathsf{A}(\mathsf{B})$ for some B. In such a case, the combinatorics of the renormalized map $\mathcal{R}_\mathsf{A}(f)$ is $\mathsf{K}(\mathcal{R}_\mathsf{A}(f)) = \mathsf{B}$:

$$\mathsf{K}(f) = \mathscr{C}_\mathsf{A}(\mathsf{B}) \quad \Rightarrow \quad \mathsf{K}(\mathcal{R}_\mathsf{A}(f)) = \mathsf{B} \ . \tag{5}$$

In summary, to formulate PACSE in a particular scenario, we need to supply:

(i) a class of maps;
(ii) a combinatorial description $\mathsf{K} \in \mathscr{K}$ of some dynamical behavior that allows to select the parameters in a family;
(iii) a combinatorial transformation $\mathscr{C}_\mathsf{A} : \mathscr{K} \to \mathscr{K}$ (with $\mathsf{A} \in \mathscr{K}_0$) that increases the combinatorial complexity;
(iv) a combinatorial operation $\star$ satisfying (4);
(v) a definition of parameter-space scaling exponents δ_A (2) and spatial scaling exponents α_A (3).

2.2 Precise formulation of PACSE

We use the associativity of the composition $\star$ to introduce the notations $\mathsf{A}^{\star 1} := \mathsf{A}$ and $\mathsf{A}^{\star k} := \mathsf{A}\star\mathsf{A}^{\star(k-1)}$.

Principle of Approximate Combination of Scaling Exponents. *Within a given class of maps,*

(a) there exist positive constants C_1 and C_2 such that

$$C_1 \le \frac{\delta_{\mathsf{A}\star\mathsf{B}}}{\delta_{\mathsf{A}}\,\delta_{\mathsf{B}}} \le C_2 \quad \text{and} \quad C_1 \le \frac{\alpha_{\mathsf{A}\star\mathsf{B}}}{\alpha_{\mathsf{A}}\,\alpha_{\mathsf{B}}} \le C_2 \ ,$$

where the constants C_i depend only on some crude properties of A and B;

(b) for any A and B from $\mathscr{K}_0$, the ratios

$$\mathcal{D}_k := \frac{\delta_{\mathsf{A}^{\star k}\star\mathsf{B}}}{(\delta_{\mathsf{A}})^k\,\delta_{\mathsf{B}}} \quad \text{and} \quad \mathcal{A}_k := \frac{\alpha_{\mathsf{A}^{\star k}\star\mathsf{B}}}{(\alpha_{\mathsf{A}})^k\,\alpha_{\mathsf{B}}} \tag{6}$$

converge as $k \to \infty$;

(c) for fixed A and B, the ratios $\mathcal{D}_k$ and $\mathcal{A}_k$ in (6) approach their limiting values $\mathcal{D}_\infty$ and $\mathcal{A}_\infty$ exponentially, i.e., there exist constants $\xi_{\mathsf{A}} > 0$ and $\eta_{\mathsf{A}} > 0$ (depending only on A) such that

$$|\mathcal{D}_k - \mathcal{D}_\infty| \approx \text{const} \cdot (\xi_{\mathsf{A}})^k \ , \qquad |\mathcal{A}_k - \mathcal{A}_\infty| \approx \text{const} \cdot (\eta_{\mathsf{A}})^k \ . \tag{7}$$

As an illustration of the properties of A and B alluded to in part (a), we consider the case of quasiperiodic renormalization. In this case, the constants C_i depend only on the maximum $\max\{a_1, \dots, a_p, b_1, \dots, b_q\}$ of the partial quotients of the continued fraction expansions of the rotation numbers $\mathsf{A} = \langle (a_1 \dots a_p)^\infty \rangle$ and $\mathsf{B} = \langle (b_1 \dots b_q)^\infty \rangle$ (the notations are introduced in Section 4.2). This dependence is very mild.

3 PACSE for unimodal maps of the interval

In this section we start the description of steps (i)-(v) of the construction outlined in Section 2.1 in the particular case of unimodal maps of the interval, and the three subsequent sections contain the constructions in three other concrete scenarios.

3.1 Definitions from kneading theory

We consider unimodal maps f from the interval $[-1, 1]$ to itself that satisfy the following conditions: $f \in C([-1, 1])$, $f \in C^3((-1, 1))$, $f' > 0$ on $[-1, 0)$, $f' < 0$ on $(0, 1]$, $f(0) = 1$, the Schwarzian derivative of f (defined, e.g., in [9, Section II.4]) is negative on $(-1, 0) \cup (0, 1)$. We will also assume that the maps are even, $f(x) = f(-x)$. It is known that this can be done without any loss of generality and simplifies several formulas.

In our numerical studies we used the 1-parameter family of maps with a quadratic maximum, $f_\mu : [0, 1] \to [0, 1]$,

$$f_\mu(x) = 1 - \mu x^2 \ , \qquad \mu \in [0, 2] \ , \tag{8}$$

and the 1-parameter family of maps with a quartic maximum, $g_\mu : [0, 1] \to [0, 1]$,

$$g_\mu(x) = 1 - \mu x^4 \ , \qquad \mu \in [0, 2] \ . \tag{9}$$

In the explanations below we will use f to denote both f_μ or g_μ.

Since we will be dealing only with superstable periodic orbits of unimodal maps, we will introduce only the tools for combinatorial description of such maps, referring the reader to [14,15] or Part II of [9] for the general case. We assume that the only critical point of the maps considered is $c = 0$ (as for the maps (8) and (9)). Let $f(0)$, $f^2(0)$, …, $f^{p-1}(0)$, $f^p(0) = 0$ be a superstable periodic orbit of f of length p. For $x \in [-1, 1]$, define

$$\mathcal{J}(x) = \begin{cases} \mathrm{L} & \text{if } x \in [-1, 0) \ , \\ \mathrm{C} & \text{if } x = 0 \ , \\ \mathrm{R} & \text{if } x \in (0, 1] \ . \end{cases}$$

Then the *kneading sequence* A of f is defined as the sequence of $(p-1)$ symbols L or R

$$\mathsf{A} = \left(\mathcal{J}(f(0)), \mathcal{J}(f^2(0)), \ldots, \mathcal{J}(f^{p-1}(0))\right) .$$

By definition, the *length*, $|\mathsf{A}|$, of this kneading sequence is p, the length of the superstable periodic orbit (although A consists of $(p-1)$ symbols). If $f^j(0) \neq 0$ for any $j \in \mathbb{N}$, then the kneading sequence of a map f is defined as the infinite sequence $\left(\mathcal{J}(f(0)), \mathcal{J}(f^2(0)), \mathcal{J}(f^3(0)), \ldots\right)$ of L's and R's.

The assumption that the Schwarzian derivative of f is negative guarantees that the orbit that realizes the kneading sequence is unique [55] (see also [9, Section II.4]). Let μ_{A} be the value for which $f_{\mu_{\mathsf{A}}}$ has a superstable periodic orbit with kneading sequence A; for brevity, we will write f_{A} for $f_{\mu_{\mathsf{A}}}$. Clearly, $f_{\mathsf{A}}^{|\mathsf{A}|}(0) = 0$ and $\left(f_{\mathsf{A}}^{|\mathsf{A}|}\right)'(0) = 0$.

The composition operation $\star$ (4) in the set of kneading sequences is usually denoted by $*$. It was introduced in [14] as follows. Let $\mathsf{AB} = a_1 a_2 \ldots a_{p-1} b_1 b_2 \ldots b_{q-1}$ stand for the *concatenation* of the kneading sequences $\mathsf{A} = a_1 a_2 \ldots a_{p-1}$ and $\mathsf{B} = b_1 b_2 \ldots b_{q-1}$ (where a_i and b_i are L's or R's); and let $\mathsf{A}^k := \mathsf{AA}\cdots\mathsf{A}$ (k copies). Then $\mathsf{A} * \mathsf{B}$ (of length $|\mathsf{A} * \mathsf{B}| = pq$) is defined as follows (for $|\mathsf{A}| \geq 2$):

- if A contains an even number of symbols R, then $\mathsf{A} * \mathsf{B} := \mathsf{A}b_1\mathsf{A}b_2\mathsf{A}\cdots\mathsf{A}b_{q-1}\mathsf{A}$;
- if A contains an odd number of symbols R, then $\mathsf{A} * \mathsf{B} := \mathsf{A}\check{b}_1\mathsf{A}\check{b}_2\mathsf{A}\cdots\mathsf{A}\check{b}_{q-1}\mathsf{A}$, where $\check{\mathrm{L}} = \mathrm{R}$, $\check{\mathrm{R}} = \mathrm{L}$.

The $*$ operation is associative, but not commutative, as mentioned in Section 2.1.

In the notations of Section 2.1, $\mathscr{K}$ is the set of all kneading sequences (finite or infinite), while $\mathscr{K}_0$ is the set of all finite kneading sequences.

The importance of the $*$ composition law is that it creates a more complicated kneading sequence $\mathsf{A} * \mathsf{B}$ from two simpler kneading sequences A and B, embedding the dynamics of B into the dynamics of A, so that A describes the large-scale dynamics and B describes the small-scale dynamics (embedded in the dynamics of A) of the map $f_{\mathsf{A}*\mathsf{B}}$. In other words, one can decompose the superstable orbit of $f_{\mathsf{A}*\mathsf{B}}$ (of length $|\mathsf{A}||\mathsf{B}|$) into $|\mathsf{A}|$ clusters, each consisting of $|\mathsf{B}|$ adjacent points. Then the map $f_{\mathsf{A}*\mathsf{B}}$ acting on the clusters has dynamics described by A. Within each cluster, the iterated map $f_{\mathsf{A}*\mathsf{B}}^{|\mathsf{A}|}$ has dynamics given by the sequence B. For an example, see [15, p. 273].

The $*$ operation reveals the *internal similarity* of the set of all kneading sequences, i.e., the fact that there exists an order-preserving map (for the definition of the ordering see the references cited above) of the set of all kneading sequences $\mathscr{K}$ into one of its subsets: $\mathscr{C}_{\mathsf{A}} : \mathscr{K} \to \mathscr{K} : \mathsf{B} \mapsto \mathscr{C}_{\mathsf{A}}(\mathsf{B}) := \mathsf{A} * \mathsf{B}$ as discovered in [14].

We note that a unimodal map f is in the domain of the renormalization operator $\mathcal{R}_{\mathsf{A}}$ if and only if its keading sequence can be written $\mathsf{K}(f) = \mathsf{A} * \mathsf{B}$, then, according to (5), we have $\mathsf{K}(\mathcal{R}_{\mathsf{A}}(f)) = \mathsf{B}$, so that the renormalized map $\mathcal{R}_{\mathsf{A}}(f)$ may fail to be renormalizable. One can think that the renormalization operator $\mathcal{R}_{\mathsf{A}}$ is expanding in the combinatorics because it maps a very reduced domain (the kneading sequences of the form $\mathsf{A} * \mathsf{B}$ for arbitrary B) onto all the kneading sequences.

In the notations introduced above, the universality discovered by Feigenbaum-Coullet-Tresser [18,19, 62] corresponds to one particular sequence of kneading sequences, namely, R^{*k}, $k \in \mathbb{N}$. PACSE generalizes this for all cascades of kneading sequences of the form $\mathsf{A}^{*k} * \mathsf{B}$, $k \in \mathbb{N}$.

3.2 Scaling exponents and renormalization operators for unimodal maps

Following [15], we define below scaling exponents for unimodal maps. By "order of the maximum" we mean the order of the first term in the Taylor expansion of $[f_\mu(x) - f_\mu(0)]$ around its maximum $c = 0$. We will focus on orders 2, a quadratic maximum [18,19,62], and 4, a quartic maximum [63]. We will assume that all maps in a family have the same order of their maximum.

For a given family f_μ, given kneading sequences A and B, and for each $k \in \{0, 1, 2, \ldots\}$, the map $f_{\mathsf{A}^{*k}*\mathsf{B}}^{|\mathsf{A}|^k}$ has a superstable periodic orbit of period $|\mathsf{B}|$. The key numerical observation of [18,19,62,15] is that the maps $f_{\mathsf{A}^{*k}*\mathsf{B}}^{|\mathsf{A}|^k}$, appropriately rescaled, converge as $k \to \infty$. More precisely, if $\beta_{\mathsf{A}^{*k}*\mathsf{B}} := \left[f_{\mathsf{A}^{*k}*\mathsf{B}}^{|\mathsf{A}|^k}(0)\right]^{-1}$, then the maps $\beta_{\mathsf{A}^{*k}*\mathsf{B}}\, f_{\mathsf{A}^{*k}*\mathsf{B}}^{|\mathsf{A}|^k}\left(\dfrac{x}{\beta_{\mathsf{A}^{*k}*\mathsf{B}}}\right)$ (each of which has a superstable periodic orbit of period $|\mathsf{B}|$) converge as $k \to \infty$. The ratios of two consecutive rescaling constants, $\frac{\beta_{\mathsf{A}^{*(k+1)}*\mathsf{B}}}{\beta_{\mathsf{A}^{*k}*\mathsf{B}}}$, also converge to a constant α_{A}^{-1} depending only on A (and the order of the maximum of the family). Led by this observation, one can

define a renormalization operator $\mathcal{R}_{\mathsf{A}}$ as follows:

$$(\mathcal{R}_{\mathsf{A}} f)(x) = \beta_f \, f^{|\mathsf{A}|}\left(\frac{x}{\beta_f}\right) \ ,$$

where β_f is the appropriate rescaling constant (recall that we are considering only even maps; otherwise, one would have to consider including a sign in the definition).

Scaling exponents corresponding to A with $|\mathsf{A}| \geq 3$ are much less popular than the ones coming from the first period-doubling cascade R^{*k}. The reasons for this are perhaps that they occur for parameter values greater than $\mu_{\mathsf{R}^{*\infty}}$, and that they are not adjacent in the bifurcation diagram. Nevertheless, they have been computed by several authors ([15], [7], [56], among others), and have even found their place in the collection of mathematical constants in [21].

Now we are ready to define the scaling exponents for unimodal maps. To avoid repetition, we will always talk about maps with the same order of their maxima, and will not write the order of the maximum in the notation for the scaling exponents, except in the tables with the numerical values of these exponents.

(a) **Parameter-space scaling exponent** δ_{A}. If $\mu_{\mathsf{A}^{*k}*\mathsf{B}}$ stands for the value of the parameter for which the map has a superstable periodic orbit, then

$$\delta_{\mathsf{A}}^{-1} := \lim_{k\to\infty} \frac{\mu_{\mathsf{A}^{*(k+1)}*\mathsf{B}} - \mu_{\mathsf{A}^{*k}*\mathsf{B}}}{\mu_{\mathsf{A}^{*k}*\mathsf{B}} - \mu_{\mathsf{A}^{*(k-1)}*\mathsf{B}}} \ ,$$

where δ_{A} is universal, i.e., depending only on A and the order of the maximum of the map, but is otherwise independent of the map f when the maps range over a small enough neighborhood.

(b) **Configuration-space (real-space) scaling exponent** α_{A} is defined as the limiting value of the ratio of two consecutive rescaling factors defined above:

$$\alpha_{\mathsf{A}}^{-1} := \lim_{k\to\infty} \frac{\beta_{\mathsf{A}^{*(k+1)}*\mathsf{B}}}{\beta_{\mathsf{A}^{*k}*\mathsf{B}}} \ ;$$

α_{A} is universal (in the same sense as for δ_{A}).

3.3 Numerical methods for the scaling exponents of unimodal maps

Since the ideas used to compute the values of the scaling exponents are the same for the families f_μ (8) and g_μ (9), below we use f_μ as an example.

The main task is to find the value of the parameter μ_{A} for which the map f_μ has superstable periodic orbit with kneading sequence $\mathsf{A} = a_1 a_2 \ldots a_{p-1}$. Since for our maps the critical point c is always 0, this means that we are looking for μ_{A} for which 0 belongs to a periodic orbit of length p such that the iterates of 0 follow the sequence A, i.e., for $j = 1, 2, \ldots, p-1$,

$$f_{\mu_{\mathsf{A}}}^{j}(0) \in \begin{cases} [-1, 0) & \text{if } a_j = \mathrm{L} \\ (0, 1] & \text{if } a_j = \mathrm{R} \ . \end{cases}$$

We define two inverses, $f_\mu^{-1,\mathrm{L}}$ and $f_\mu^{-1,\mathrm{R}}$, of the map f_μ:

$$f_\mu^{-1,\mathrm{L}}(y) := -\sqrt{\frac{1-y}{\mu}} \quad \text{and} \quad f_\mu^{-1,\mathrm{R}}(y) := +\sqrt{\frac{1-y}{\mu}} \ , \qquad \text{for } y < 1 \ .$$

With this notation, μ_{A} must satisfy the equation

$$f_\mu^{-1,a_1} \circ f_\mu^{-1,a_2} \circ \ldots \circ f_\mu^{-1,a_{n-2}} \circ f_\mu^{-1,a_{n-1}}(0) = f(0) = 1 \ .$$

Taking f_μ of both sides and noticing that $f_\mu(1) = 1 - \mu$, we see that μ_{A} must satisfy

$$\Phi(\mu) := f_\mu^{-1,a_2} \circ \ldots \circ f_\mu^{-1,a_{n-2}} \circ f_\mu^{-1,a_{n-1}}(0) - 1 + \mu = 0 \ .$$

To solve the equation $\Phi(\mu) = 0$ with high accuracy, we used the Brent zero-finding algorithm [4, Chapter 4]. This method is quadratically convergent, so it is practical even for calculations with several hundred digits. At the same time, it brackets the solution, so that we always know that the interval we consider contains a solution. We implemented the above algorithm by using GMP – the freely available GNU

Multiple Precision Arithmetic Library [1] which allows numerical computations with arbitrary accuracy. We performed the computations using about 600 decimal digits of accuracy.

Using this method, we found the values of $\mu_{\mathsf{A}^{*n}}$ for several n, and used them to compute the ratios $\frac{\mu_{\mathsf{A}^{*(n+1)}}-\mu_{\mathsf{A}^{*n}}}{\mu_{\mathsf{A}^{*n}}-\mu_{\mathsf{A}^{*(n-1)}}}$. If this could be done for several values of n, we used multiple Aitken's extrapolation to find the value of δ_{A}. To compute the values of α_{A}, we found the scaling of the closest returns of the orbit of the critical point to itself, which is similar to the definition of the configuration-space scaling exponent for the case of circle maps (see equation (11) below). In principle, if $\mu_{\mathsf{A}^{*\infty}} = \lim_{n\to\infty} \mu_{\mathsf{A}^{*n}}$, then one can study the closest returns to the critical point of the orbit of the critical point under the map $f_{\mu_{\mathsf{A}^{*\infty}}}$, which occur if the map is iterated $|\mathsf{A}^{*n}|$ times. If $d_n := \left| f^{|\mathsf{A}^{*n}|}_{\mu_{\mathsf{A}^{*\infty}}}(0) - 0 \right|$ are these closest returns, then α_{A} is computed from $\alpha_{\mathsf{A}}^{-1} = \lim_{n\to\infty} \frac{d_n}{d_{n-1}}$ (compare this with the definition (11) of the configuration-space scaling exponent for circle maps). In practice, instead of using $\mu_{\mathsf{A}^{*\infty}}$, we computed $\mu_{\mathsf{A}^{*N}}$ for some large N, and then used this value instead of $\mu_{\mathsf{A}^{*\infty}}$ in the computations of the closest returns d_n. In the numerical example in Table 1 below, we took $N = 10$, computed $d_1, \ldots, d_9$, and used these ratios to find α_{A}. As one can see from the table, as n increases, the ratios $\frac{d_{n-1}}{d_n}$ first start stabilizing, but when n approaches $N = 10$, the convergence seems to break down. This is easy to explain – in the computation of d_n, we should have used the exact value $\mu_{\mathsf{A}^{*\infty}}$ instead of the approximate one, $\mu_{\mathsf{A}^{*N}}$. This introduces a small error for low iterates, but is fatal for high ones.

3.4 Numerical results on PACSE for unimodal maps

We performed numerical computations of the scaling exponents $\delta^{(2)}_{\mathsf{A}}$ and $\alpha^{(2)}_{\mathsf{A}}$ for the family f_μ (8) of unimodal maps with a quadratic maximum, and the scaling exponents $\delta^{(4)}_{\mathsf{A}}$ and $\alpha^{(4)}_{\mathsf{A}}$ for the family g_μ (9) of unimodal maps with a quartic maximum.

A major problem in our computations was the extremely fast growth of the length of the kneading sequences we needed to use in order to compute the scaling exponents. For example, to compute $\delta^{(2)}_{\mathsf{A}^{*k}*\mathsf{B}}$ for some $k \in \mathbb{N}$, we need to find the parameter values $\mu^{(2)}_{(\mathsf{A}^{*k}*\mathsf{B})^{*n}*\mathsf{C}}$ for several $n \in \mathbb{N}$ and some (arbitrary) kneading sequence C (for the family f_μ). But the length of the kneading sequence $(\mathsf{A}^{*k} * \mathsf{B})^{*n} * \mathsf{C}$ is $(|\mathsf{A}|^k|\mathsf{B}|)^n|\mathsf{C}|$, which grows very fast with n even for small $|\mathsf{A}|$. Using several tricks of indirect referencing, we were able to do computations for kneading sequences of length several billions.

In Table 1 we illustrate the process of obtaining the value of the scaling exponents $\delta^{(2)}_{\mathrm{RL}*\mathrm{R}}$ and $\alpha^{(2)}_{\mathrm{RL}*\mathrm{R}}$. The computation took several hours in a current desktop computer. The values of the parameters $\mu^{(2)}_{\mathsf{A}^{*n}}$ were computed with accuracy about 200 decimal digits, but since Table 1 is only for illustrative purposes, the values given in the table are truncated.

Table 1 Illustration for the computations of $\delta^{(2)}_{\mathrm{RL}*\mathrm{R}}$ and $\alpha^{(2)}_{\mathrm{RL}*\mathrm{R}}$; $\mathsf{A} = \mathrm{RL} * \mathrm{R} = \mathrm{RLLRL}$, $|\mathsf{A}| = |\mathrm{RL} * \mathrm{R}| = 6$.

n	$\lvert\mathsf{A}^{*n}\rvert = \lvert\mathsf{A}\rvert^n$	$\mu^{(2)}_{\mathsf{A}^{*n}}$	$\frac{\mu^{(2)}_{\mathsf{A}^{*n}} - \mu^{(2)}_{\mathsf{A}^{*(n-1)}}}{\mu^{(2)}_{\mathsf{A}^{*(n+1)}} - \mu^{(2)}_{\mathsf{A}^{*n}}}$	$d_n := \left\lvert f^{\lvert\mathsf{A}^{*n}*\mathsf{B}\rvert}_{\mu^{(2)}_{\mathsf{A}^{*10}}}(0) - 0 \right\rvert$	$\frac{d_{n-1}}{d_n}$
1	6	1.7728929033816237994341		$3.0137075740399 \times 10^{-2}$	
2	36	1.781178707403057813661 8	218.4825169765562	$1.4377337517394 \times 10^{-3}$	20.963144712
3	216	1.781216631737398593450 3	218.4160488238348	$6.8695738489866 \times 10^{-5}$	20.929029074
4	1,296	1.781216805370858886324 5	218.4118631956149	$3.2823832718048 \times 10^{-6}$	20.928616069
5	7,776	1.781216806165840705317 3	218.4117960517258	$1.5683712952838 \times 10^{-7}$	20.928610987
6	46,656	1.781216806169480535369 4	218.4117951520684	$7.4939101336644 \times 10^{-9}$	20.928610875
7	279,936	1.781216806169497200357 9	218.4117951406393	$3.5807009726033 \times 10^{-10}$	20.928600279
8	1,679,616	1.781216806169497276658 7	218.4117951404967	$1.7108927323015 \times 10^{-11}$	20.926283815
9	10,077,696	1.781216806169497277008 0	218.4117951404949	$8.1548635942729 \times 10^{-13}$	19.980028819
10	60,466,176	1.781216806169497277009 6		0	

Table 2 displays the values of the scaling exponents of the quadratic unimodal family f_μ (8). The column "Max length used" gives the maximum length of the kneading sequence used in the computations of the particular scaling exponents. Although it was often difficult to estimate the error in our

computations, we believe that the error of most of the numerical values does not exceed 2 in the last significant digit, unless indicated otherwise; (±?) means that the error could not be estimated. We also obtained the following values of the scaling exponents for the family f_μ (8) that were needed to compute the ratios of the scaling exponents in Table 4 below: $\delta^{(2)}_{\mathrm{R}} = 4.66920160910299$, $\delta^{(2)}_{\mathrm{RL}} = 55.247026588672$, $\delta^{(2)}_{\mathrm{RLL}} = 981.594976534071$, $\alpha^{(2)}_{\mathrm{R}} = 2.50290787509590$, $\alpha^{(2)}_{\mathrm{RL}} = 9.2773411156$, $\alpha^{(2)}_{\mathrm{RLL}} = 38.81907429719690$.

Table 2 Scaling exponents for the quadratic unimodal family f_μ (8).

A	B	k	Max length used	$\delta^{(2)}_{\mathsf{A}*k*\mathsf{B}}$	$\alpha^{(2)}_{\mathsf{A}*k*\mathsf{B}}$
R	RL	1	$6^{10} = 60{,}466{,}176$	218.411795140495	20.9286109
R	RL	2	$12^7 = 35{,}831{,}808$	1071.42166411881	53.468926
R	RL	3	$24^5 = 7{,}962{,}624$	5002.0407	133.7057
R	RL	4	$48^4 = 5{,}308{,}416$	23384	334.80
R	RL	5	$96^3 = 884{,}736$	109200 (±?)	837 (±?)
R	RLL	1	$8^9 = 134{,}217{,}728$	2304.55784444859	66.38970
R	RLL	2	$16^6 = 16{,}777{,}216$	12355.7086904746164	176.757
R	RLL	3	$32^4 = 1{,}048{,}576$	57319.69 ± 0.10	440.332
R	RLL	4	$64^3 = 262{,}144$	268400	1102.32 (±?)
R	RLL	5	$128^3 = 2{,}097{,}152$	1253400 (±?)	2761 (±?)
RL	R	1	$6^{10} = 60{,}466{,}176$	218.411795140495	20.9286109
RL	R	2	$18^6 = 34{,}012{,}224$	12389.010675300	196.582
RL	R	3	$54^4 = 8{,}503{,}056$	683380 ± 10	1822.35
RL	R	4	$162^3 = 4{,}251{,}528$	37760000 ± 30000	16907 (±?)
RL	RLL	1	$12^7 = 35{,}831{,}808$	49344.980718870504	343.029984
RL	RLL	2	$36^4 = 1{,}679{,}616$	2745043.1	3193.15
RL	RLL	3	$108^3 = 1{,}259{,}712$	151586000 ± 4000	29616 (±?)

Table 3 shows the computed values of the scaling exponents of the quartic unimodal family g_μ (9). The notations are the same as in Table 2. We also obtained the following values of the scaling exponents for the family (9) that were needed to compute the ratios in Table 4 below: $\delta^{(4)}_{\mathrm{R}} = 7.2846862170733434$, $\delta^{(4)}_{\mathrm{RL}} = 85.7916290913561$, $\delta^{(4)}_{\mathrm{RL}} = 1275.1129946531598071$, $\alpha^{(4)}_{\mathrm{R}} = 1.69030297$; $\alpha^{(4)}_{\mathrm{RL}} = 3.15215735$; $\alpha^{(4)}_{\mathrm{RLL}} = 6.191800569$.

Table 3 Scaling exponents for the quartic unimodal family g_μ (9).

A	B	k	Max length used	$\delta^{(4)}_{\mathsf{A}*k*\mathsf{B}}$	$\alpha^{(4)}_{\mathsf{A}*k*\mathsf{B}}$
R	RL	1	$6^{10} = 60{,}466{,}176$	465.2710814026	4.93533166
R	RL	2	$12^7 = 35{,}831{,}808$	3615.136820	8.47054
R	RL	3	$24^5 = 7{,}962{,}624$	26031.25	14.2755
R	RL	4	$48^4 = 5{,}308{,}416$	190000 ± 20	24.1707
R	RL	5	$96^3 = 884{,}736$	1380000 (±?)	39.8 (±?)
R	RLL	1	$8^9 = 134{,}217{,}728$	3306.0917724	8.03318
R	RLL	2	$16^6 = 16{,}777{,}216$	29689.5614	14.2896
R	RLL	3	$32^4 = 1{,}048{,}576$	207679.9	23.9058
R	RLL	4	$64^3 = 262{,}144$	1523400 (±?)	40.475 (±?)
R	RLL	5	$128^3 = 2{,}097{,}152$	11080000 (±?)	68.38 (±?)
RL	R	1	$6^{10} = 60{,}466{,}176$	465.2710814026	4.93533166
RL	R	2	$18^6 = 34{,}012{,}224$	43008.44 ± 0.04	15.845786 ± 0.000005
RL	R	3	$54^4 = 8{,}503{,}056$	3644000	49.79 (±?)
RL	R	4	$162^3 = 4{,}251{,}528$	313000000 (±?)	157 (±?)
RL	RLL	1	$12^7 = 35{,}831{,}808$	91623.170130	18.6618
RL	RLL	2	$36^4 = 1{,}679{,}616$	8112000	59.29 (±?)
RL	RLL	3	$108^3 = 1{,}259{,}712$	692000000 (±?)	186 (±?)

Table 4 shows the ratios

$$\mathcal{D}_k^{(d)} = \frac{\delta_{\mathsf{A}^{*k}*\mathsf{B}}^{(d)}}{\left(\delta_{\mathsf{A}}^{(d)}\right)^k \delta_{\mathsf{B}}^{(d)}} \quad \text{and} \quad \mathcal{A}_k^{(d)} = \frac{\alpha_{\mathsf{A}^{*k}*\mathsf{B}}^{(d)}}{\left(\alpha_{\mathsf{A}}^{(d)}\right)^k \alpha_{\mathsf{B}}^{(d)}}\,, \qquad d = 2, 4$$

for the data from Tables 2 and 3. These ratios provide numerical evidence for parts (a) and (b) of PACSE for unimodal maps. The fact that the ratios $\mathcal{D}_k^{(d)}$ and $\mathcal{A}_k^{(d)}$ seem to converge as $k \to \infty$ is even more striking if one takes into account that some of the exponents used to compute these ratios were very large – up to several hundred million! Part (c) of PACSE cannot be seen from these tables because of the extremely fast growth of the length of the kneading sequences. We will show numerical evidence for the exponential rate of convergence of $\mathcal{D}_k^{(d)}$ and $\mathcal{A}_k^{(d)}$ in other cases – critical (Section 4.4) and non-critical (Section 4.5) circle maps, and dynamics on the boundary of Siegel disks (Section 5.2).

Table 4 Ratios of the scaling exponents (5.2) for the quadratic ($d = 2$) and quartic ($d = 4$) unimodal families.

A	B	k	$\mathcal{D}_k^{(2)}$	$\mathcal{A}_k^{(2)}$	$\mathcal{D}_k^{(4)}$	$\mathcal{A}_k^{(4)}$
R	RL	1	0.846690238310410	0.90130548	0.744475304148	0.92628344
R	RL	2	0.889541596766076	0.920000801	0.7940687858	0.940533
R	RL	3	0.88942725	0.9191614	0.7849058	0.937756
R	RL	4	0.89052	0.91956	0.78644	0.93934
R	RL	5	0.8907 (±?)	0.918 (±?)	0.784 (±?)	0.915 (±?)
R	RLL	1	0.50282013432097	0.683299	0.35592245110	0.767549
R	RLL	2	0.57736450402003890	0.72684	0.438766449	0.807744
R	RLL	3	0.5736455	0.723437	0.4213211	0.799452
R	RLL	4	0.5753 ± 0.0005	0.72357	0.42425 (±?)	0.80078 (±?)
R	RLL	5	0.5754 (±?)	0.7241 (±?)	0.4236 (±?)	0.8004 (±?)
RL	R	1	0.846690238310410	0.90130548	0.744475304148	0.92628344
RL	R	2	0.8693130162750	0.91254	0.8021445	0.9434816
RL	R	3	0.86794	0.911835	0.7922	0.9404 (±?)
RL	R	4	0.8681 ± 0.0007	0.91186 (±?)	0.793 (±?)	0.941 (±?)
RL	RLL	1	0.9099169335611600	0.9524964880	0.83755189927	0.956156
RL	RLL	2	0.9162184	0.955712	0.8643	0.9637 (±?)
RL	RLL	3	0.91580	0.95546 (±?)	0.859 (±?)	0.959 (±?)

4 PACSE for for circle maps

4.1 Preliminaries

We start with a brief collection of definitions and facts about circle maps (for details see, e.g., [30, Ch. 11, 12] or [44, Ch. 1]). Let $\mathbb{T} = \mathbb{R}/\mathbb{Z}$ stand for the circle and $\pi : \mathbb{R} \to \mathbb{T} : x \mapsto \pi(x) := x \bmod 1$. If $F : \mathbb{R} \to \mathbb{R}$ is a map satisfying $F(x + 1) = F(x) + 1$, then the map $f : \mathbb{T} \to \mathbb{T}$ that satisfies $f \circ \pi = \pi \circ F$ is a map of the circle $\mathbb{T}$, and F is called a *lift* of f. We will always assume that f is an orientation-preserving homeomorphism. The *rotation number* of f is defined as

$$\tau(f) := \left(\lim_{n\to\infty} \frac{F^n(x) - x}{n}\right) \bmod 1;$$

$\tau(f)$ exists and is independent of the choice of F and $x \in \mathbb{T}$.

Two circle maps f and g are *topologically* (respectively C^k*, smoothly, analytically*) *conjugate* if there exists a homeomorphism (respectively C^k, C^∞, analytic diffeomorphism) h of the circle such that $f = h^{-1} \circ g \circ h$. The map h is called the *conjugacy* between f and g. If the $\tau(f)$ is irrational and the orbit of some point is dense in $\mathbb{T}$, then f is topologically conjugate to the *rigid rotation* $r_{\tau(f)} : \mathbb{T} \to \mathbb{T} : x \mapsto (x + \tau(f)) \bmod 1$.

There is a multitude of results concerning the regularity of the conjugacy h between f and $r_{\tau(f)}$ [3, 45,29,54,31,68,66,57,33] (the proofs in [54,57,33] used renormalization ideas). These regularity results guarantee that if f is a regular enough circle diffeomorphism with rotation number that is Diophantine, then f is smoothly conjugate to a rigid rotation (the regularity of the conjugacy depends on the regularity

of f and the Diophantine properties of $\tau(f)$). One immediate consequence of this is that the scaling exponents of a family of circle diffeomorphisms and the corresponding family of rigid rotations are the same; we use this fact in Section 4.5 to find explicit expressions for the scaling exponents in this case.

An important topic in the theory of circle maps is the dynamical behavior of *critical* circle maps, i.e., analytic circle homeomorphisms that have a critical point c at which $f'(c) = 0$. Obviously, the Taylor expansion of such a map around c has the form $f(x) = f(c) + \frac{1}{n!}f^{(n)}(c)(x-c)^n + \cdots$, where $n = 3$ (*cubic critical*), 5 (*quintic critical*), ... In [67] it is shown that these maps are topologically conjugate to rotations. Clearly, the conjugacy h cannot even be Lipschitz. The Hölder regularity of the conjugacy was investigated numerically by two of the authors of the present paper in [37], where one can find many references on critical circle maps and their conjugacies.

4.2 Rotation numbers – notations

Let $\mathsf{A} = (a_1, a_2, \ldots, a_p)$ be a sequence of p natural numbers $a_j \in \mathbb{N}$; we will usually omit the commas and write $\mathsf{A} = (a_1 a_2 \ldots a_p)$. Let $|\mathsf{A}| = p$ be the length of A. If $\mathsf{B} = (b_1 b_2 \ldots b_q)$ is another such sequence, let $\mathsf{AB} := (a_1 a_2 \ldots a_p b_1 b_2 \ldots b_q)$ stand for the *concatenation* of A and B. Let AB^n denote the sequence $\mathsf{ABB}\cdots\mathsf{B}$ (B repeated n times), and $\mathsf{AB}^\infty := \mathsf{ABB}\cdots$. Denote by

$$\langle \mathsf{B} \rangle = \langle b_1 b_2 \ldots b_q \rangle := \cfrac{1}{b_1 + \cfrac{1}{b_2 + \cfrac{1}{\ddots + \cfrac{1}{b_q}}}}$$

the continued fraction expansion (CFE) whose partial quotients are the numbers constituting B; the meaning of $\langle \mathsf{AB}^n \rangle := \langle \mathsf{ABB}\cdots\mathsf{B} \rangle$ is analogous, and $\langle \mathsf{AB}^\infty \rangle := \lim_{n\to\infty} \langle \mathsf{AB}^n \rangle$. Let $\mathcal{G} : (0,1) \to (0,1)$ be the *Gauss map*,

$$\mathcal{G}(x) := \frac{1}{x} - \left\lfloor \frac{1}{x} \right\rfloor ,$$

which satisfies $\mathcal{G}(\langle a_1 a_2 \cdots a_n \cdots \rangle) = \langle a_2 \cdots a_n \cdots \rangle$.

We are especially interested in studying numbers with CFEs of the form

$$\langle \mathsf{HT}^\infty \rangle := \lim_{n\to\infty} \langle \mathsf{HT}^n \rangle ,$$

which are called *eventually periodic*. A number is of this type if and only if it is a root of a quadratic equation with integer coefficients (see [28, Theorems 176 and 177]), so such numbers are also called *quadratic irrationals*. We will call H the *head* and T^∞ the *tail*, T the *periodic part*, and $|\mathsf{T}|$ the *length* of the periodic part of the CFE. Clearly, after removing the head H by applying the Gauss map $|\mathsf{H}|$ times, the resulting number $\mathcal{G}^{|\mathsf{H}|}(\langle \mathsf{HT}^\infty \rangle) = \langle \mathsf{T}^\infty \rangle$ is periodic for the Gauss map: $\mathcal{G}^{|\mathsf{T}|}(\langle \mathsf{T}^\infty \rangle) = \langle \mathsf{T}^\infty \rangle$. If two quadratic irrationals have the same tail, they are said to be *equivalent*.

4.3 Scaling exponents and renormalization for circle maps

To define the scaling exponents for circle maps, consider the archetypal circle map,

$$f_{\omega,\gamma}(x) = (x + \omega + \gamma g(x)) \bmod 1 ,$$

where g is a 1-periodic analytic function. We will be interested mainly in critical maps, in which case we assume that there exists only one point $c \in \mathbb{T}$ for which $f'_{\omega,\gamma}(c) = 1 + \gamma g'(c) = 0$. Assume also that the rotation number of the map is eventually periodic: $\tau(f_{\omega,\gamma}) = \langle \mathsf{HT}^\infty \rangle \in (0,1) \setminus \mathbb{Q}$. For a fixed value of γ, define the *phase locking intervals*, $I_n(\gamma)$, as the intervals of the parameter ω for which the rotation number of the map is equal to the rational approximant $\frac{P_n}{Q_n} = \langle \mathsf{HT}^n \rangle$ of the rotation number (hence, the map has a periodic orbit of period Q_n):

$$I_n(\gamma) := \left\{ \omega \in (0,1) \ : \ \tau(f_{\omega,\gamma}) = \frac{P_n}{Q_n} \right\} .$$

Since $\langle \mathsf{HT}^\infty \rangle$ is irrational, the iterates of every point $x \in \mathbb{T}$ fill the circle densely and never come back to x, but $\lim_{n\to\infty} f^{Q_n}(x) = x$. Now we are ready to define the scaling exponents for a circle map f with one critical point c.

(a) **Parameter-space scaling exponent** δ_{T}. For a given value of γ, the lengths $|I_n(\gamma)|$ of the phase-locking intervals scale as

$$|I_n(\gamma)| \approx C\delta_{\mathsf{T}}^{-n} \ , \tag{10}$$

where δ_{T} is a universal number, i.e., a number that depends only on T and the order of the critical point c, but is otherwise independent of the map f when the maps range over a small enough neighborhood.

(b) **Configuration-space scaling exponent** α_{T}**.** For a critical circle map with rotation number $\langle \mathsf{HT}^\infty \rangle$, the rate at which the iterates of the critical point c return to it is given by

$$|f^{Q_n}(c) - c| \approx C\alpha_{\mathsf{T}}^{-n} \ , \tag{11}$$

where α_{T} is a universal number (in the same sense as for δ_{T}).

Since the scaling exponents depend on the order of the critical point, we will put a superscript to indicate the order, using N for non-critical, C for cubic critical, and Q for quintic critical maps. In the notations above we tacitly assumed that the scaling exponents depend only on the tail T of $\langle \mathsf{HT}^\infty \rangle$ – this fact is one of the consequences of the existence of renormalization group.

The scaling exponents for cubic critical circle maps were introduced in [51], where it was found that for rotation numbers of the form $\langle \mathsf{H1}^\infty \rangle$ these scaling exponents do not depend on the particular map and on the head H. Soon after that, a renormalization operator acting on critical circle maps was constructed (at a "physical" level of rigor) in [50] and [20] in order to explain the findings of [51].

4.4 PACSE for circle maps – formulation, numerical methods and results

PACSE for circle maps is a particular case of the general formulation given in Section 2.2; we only need to specify that for circle maps, the operation $*$ (4) is defined as concatenation:

$$\mathsf{A} * \mathsf{B} = \mathsf{AB} \ , \qquad \mathsf{A}^{*k} * \mathsf{B} = \mathsf{A}^k\mathsf{B} \ . \tag{12}$$

In these notations, for example, $\delta^{\mathrm{C}}_{\mathsf{A}^k\mathsf{B}}$ is the universal number that comes from studying the lengths of the phase-locking intervals $I_n(\gamma)$ (10) for a cubic critical map with rotation numbers $\langle \mathsf{H}(\mathsf{A}^k\mathsf{B})^n \rangle$, $n \in \mathbb{N}$ (the scaling exponents do not depend on the head H).

The formulation of PACSE for circle maps is a particular case of the general statement given in Section 2.2; in particular, we are interested in the behavior for large k of the ratios

$$\mathcal{D}^\bullet_k := \frac{\delta^\bullet_{\mathsf{A}^k\mathsf{B}}}{(\delta^\bullet_{\mathsf{A}})^k\,\delta^\bullet_{\mathsf{B}}} \quad \text{and} \quad \mathcal{A}^\bullet_k := \frac{\alpha^\bullet_{\mathsf{A}^k\mathsf{B}}}{(\alpha^\bullet_{\mathsf{A}})^k\,\alpha^\bullet_{\mathsf{B}}} \ , \qquad \bullet = \mathrm{N},\ \mathrm{C},\ \mathrm{Q} \ . \tag{13}$$

To compute the parameter-space scaling exponents for rotation numbers of the form $\langle \mathsf{T}^\infty \rangle$ for $\mathsf{T} = (t_1 t_2 \dots t_p)$ (with $t_j \in \mathbb{N}$), we used the following method (similar to the one two of the autors of the present paper used in [37]). Let $f_{\omega,\beta}$ be the circle map and $F_{\omega,\beta}$ be its lift. Let F_n be the Fibonacci-like sequence generating $\mathsf{T} = (t_1 t_2 \dots t_p)$: $F_0 = 0$, $F_1 = 1$, $F_1/F_2 = \frac{1}{t_p + (F_0/F_1)}$, $F_2/F_3 = \frac{1}{t_{p-1} + (F_1/F_2)}$, …, and let $I_n(\beta)$ stand for the phase-locking interval where the rotation number of $f_{\omega,\beta}$ equals F_n/F_{n+1}. To find the ends of the interval $I_n(\beta)$, we used the fact that when ω enters $I_n(\beta)$, the map $x \mapsto (F_{\omega,\beta})^{F_{n+1}}(x) - F_n$ undergoes a tangent bifurcation. To determine these values, we used the subroutines FMIN and ZEROIN from [22], and the DOUBLEDOUBLE software package [5] providing about 30 decimal digits of accuracy.

In our computations we studied the following families of circle maps:

– the cubic critical (C) family ($0 \le \beta < \frac{4}{3}$, we used $\beta = 0.3$)

$$f^{\mathrm{C}}_{\omega,\beta}(x) = \Big[x + \omega - \tfrac{1}{2\pi}(\beta \sin 2\pi x + \tfrac{1-\beta}{2} \sin 4\pi x)\Big] \bmod 1 \ ,$$

where the coefficients are chosen in such a way that for every β, $f^{\mathrm{C}}_{\omega,\beta}(x) = \omega + \frac{2\pi^2(4-3\beta)}{3}x^3 + \mathcal{O}(x^5)$;

– the quintic critical (Q) family ($\frac{1}{2} \le \beta < \frac{3}{2}$, we used $\beta = 0.6$)

$$f^{\mathrm{Q}}_{\omega,\beta}(x) = \Big[x + \omega - \tfrac{1}{2\pi}(\beta \sin 2\pi x + \tfrac{9-8\beta}{10} \sin 4\pi x + \tfrac{3\beta-4}{15} \sin 6\pi x)\Big] \bmod 1 \ ,$$

where the coefficients are chosen in such a way that for every β, $f^{\mathrm{Q}}_{\omega,\beta}(x) = \omega + \frac{8\pi^4(3-2\beta)}{5} x^5 + \mathcal{O}(x^7)$;

– the maps

$$f(x) = x + \omega - \frac{b}{2\pi} \frac{\sin 2\pi x}{a - \cos 2\pi x} \tag{14}$$

with $(a, b) = (2, 1)$, for which f is cubic critical [$f(x) \approx \omega + \frac{8}{3}\pi^2 x^3 + \mathcal{O}(x^5)$]; and $(a, b) = (-2, -3)$, for which f is quintic critical [$f(x) \approx \omega + \frac{4}{45}\pi^4 x^5 + \mathcal{O}(x^7)$].
Since the maps (14) with a fixed order of critical point do not contain any free parameter, we only computed the α exponents. This was to reassure us that the results and the numerics apply to functions with infinitely harmonics. The form of the function (14) is chosen to have infinitely many harmonics with few evaluations of trigonometric functions.

We give numerical data for the scaling exponents for the C and Q cases in Tables 5 and 6, and for the ratios $\mathcal{D}_k$ and $\mathcal{A}_k$ (13) in Tables 7 and 8. In the calculations of the ratios of the exponents, we used the following computed values: $\delta^{\mathrm{C}}_1 = 2.8336106559$, $\alpha^{\mathrm{C}}_1 = 1.28857456$, $\delta^{\mathrm{Q}}_1 = 3.04337774$, $\alpha^{\mathrm{Q}}_1 = 1.193857$. To obtain each of the δ's from Tables 5 and 6, we run our programs for one-two weeks. While computing δ, we obtain with high accuracy the value of ω such that the rotation number of the circle map has the desired rotation number. Having computed this value of ω, we computed the corresponding value of α directly from the definition (11) (i.e., iterating Q_n times and measuring the closest returns); the computation of α took several hours in a desktop computer.

Although it is difficult to estimate the errors in the data, we believe that in most cases the error does not exceed 2 in the last significant digit, unless we indicate otherwise. Despite the loss of accuracy for large values of k, the ratios $\mathcal{D}_k$ and $\mathcal{A}_k$ clearly converge to some values. The existence of limits as $k \to \infty$ of $\mathcal{D}_k$ and $\mathcal{A}_k$ (as claimed by PACSE) is quite surprising since the numerical values of the configuration-space and especially of the parameter-space scaling exponents are quite large for large k – note, for example, for a quintic critical circle maps, $\delta_{1^{11}4}$ is about 14 million.

Table 5 Scaling exponents of cubic critical circle maps with rotation numbers $\langle \mathsf{T}^\infty \rangle$, $\mathsf{T} = (1^k2)$, (1^k3), and (1^k4).

	Cubic critical, $\mathsf{T} = (1^k2)$		Cubic critical, $\mathsf{T} = (1^k3)$		Cubic critical, $\mathsf{T} = (1^k4)$	
k	$\delta^{\mathrm{C}}_{1^k2}$	$\alpha^{\mathrm{C}}_{1^k2}$	$\delta^{\mathrm{C}}_{1^k3}$	$\alpha^{\mathrm{C}}_{1^k3}$	$\delta^{\mathrm{C}}_{1^k4}$	$\alpha^{\mathrm{C}}_{1^k4}$
0	6.79922516	1.58682670	13.7602824	1.85507	24.620348	2.080122
1	17.66905276	1.9691355	31.6238761	2.1741151	50.76600	2.318910
2	52.04449	2.590589	98.324667	2.9453239	165.84861	3.2192538
3	145.425152	3.308635	269.10293	3.710008	444.9945	4.005393
4	414.51561	4.28301	774.0388	4.836417	1291.564	5.25380
5	1171.7123	5.5067	2179.327	6.196286	3621.50	6.70968
6	3323.73	7.1039	6193.4	8.0082	10312	8.68597
7	9413.7	9.14860	17526	10.30338	29152	11.16593
8	26681	11.7923	49693	13.28730	82670	14.4062
9	75590	15.1929	140800	17.1147	234200	18.5514
10	214000	19.579	399000 ± 400	22.058	663000	23.913
11	607900	25.230	1131000 ± 1000	28.421	1880000 ± 4000	30.809
12	1728000 ± 3000	32.51 ± 0.01	3210000 ± 6000	36.625	5340000 ± 6000	39.705

The exponential convergence of $\mathcal{D}_k$ and $\mathcal{A}_k$ to their limits (part (c) of PACSE) is a subtle effect, but nevertheless it can be seen from our numerical data. Let $\mathcal{D}^{\mathrm{C},m}_k = \frac{\alpha^{\mathrm{C}}_{1^k m}}{(\alpha^{\mathrm{C}}_1)^k \alpha^{\mathrm{C}}_m}$, $\mathcal{A}^{\mathrm{C},m}_k = \frac{\alpha^{\mathrm{C}}_{1^k m}}{(\alpha^{\mathrm{C}}_1)^k \alpha^{\mathrm{C}}_m}$, and $\mathcal{D}^{\mathrm{C},m}_\infty$ and $\mathcal{A}^{\mathrm{C},m}_\infty$ be the corresponding limiting values as $k \to \infty$. In Figure 1 we show the plots of $|\mathcal{D}^{\mathrm{C},m}_k - \mathcal{D}^{\mathrm{C},m}_\infty|$ and $|\mathcal{A}^{\mathrm{C},m}_k - \mathcal{A}^{\mathrm{C},m}_\infty|$ for different values of m. The limiting values used in the figure were obtained from the data in Table 7 by Aitken extrapolation. The limiting values used to make the figure were the following: $\mathcal{D}^{\mathrm{C},2}_\infty = 0.94404$, $\mathcal{D}^{\mathrm{C},3}_\infty = 0.86869$, $\mathcal{D}^{\mathrm{C},4}_\infty = 0.80766$, $\mathcal{A}^{\mathrm{C},2}_\infty = 0.97756$, $\mathcal{A}^{\mathrm{C},3}_\infty = 0.94207$, $\mathcal{A}^{\mathrm{C},4}_\infty = 0.91074$. In plotting the error bars, we assumed that the absolute error in each of the values displayed in Table 7

Table 6 Scaling exponents of quintic critical circle maps with rotation numbers $\langle \mathsf{T}^\infty \rangle$, $\mathsf{T} = (1^k2)$, (1^k3), (1^k4).

	Quintic critical, $\mathsf{T} = (1^k2)$		Quintic critical, $\mathsf{T} = (1^k3)$		Quintic critical, $\mathsf{T} = (1^k4)$	
k	$\delta^{\mathrm{Q}}_{1^k2}$	$\alpha^{\mathrm{Q}}_{1^k2}$	$\delta^{\mathrm{Q}}_{1^k3}$	$\alpha^{\mathrm{Q}}_{1^k3}$	$\delta^{\mathrm{Q}}_{1^k4}$	$\alpha^{\mathrm{Q}}_{1^k4}$
0	7.7912246	1.3791501	16.71149	1.53182	31.4178	1.6478
1	21.573320	1.5985	40.26195	1.700221	66.752	1.7657
2	68.620816	1.9392	136.407	2.1057	239.4	2.2208
3	205.43	2.2997	398.36	2.4738	685	2.5901
4	629.5	2.7536	1233.2	2.9740	2134	3.123
5	1910.6	3.2836	3727.6	3.541	6435 ± 5	3.7137
6	5820	3.9216	11370	4.231	19640 ± 50	4.440
7	17710	4.6815	34590	5.0503	59700 ± 100	5.299
8	53500	5.590	105000 ± 1000	6.029	181600	6.33
9	160000	6.677	322000	7.198	570000	7.555
10	500000	7.970	990000	8.595	1750000 ± 50000	9.02
11	1600000	9.53	3100000 ± 100000	10.26	5500000 ± 300000	10.76
12	4680000 ± 50000	11.36	9500000 ± 300000	12.25	13700000 ($\pm$?)	12.8

Table 7 Ratios of the scaling exponents of cubic critical circle maps for the data from Table 5.

	Cubic critical, $\mathsf{T} = (1^k2)$		Cubic critical, $\mathsf{T} = (1^k3)$		Cubic critical, $\mathsf{T} = (1^k4)$	
k	$\dfrac{\delta^{\mathrm{C}}_{1^k2}}{(\delta^{\mathrm{C}}_1)^k\,\delta^{\mathrm{C}}_2}$	$\dfrac{\alpha^{\mathrm{C}}_{1^k2}}{(\alpha^{\mathrm{C}}_1)^k\,\alpha^{\mathrm{C}}_2}$	$\dfrac{\delta^{\mathrm{C}}_{1^k3}}{(\delta^{\mathrm{C}}_1)^k\,\delta^{\mathrm{C}}_3}$	$\dfrac{\alpha^{\mathrm{C}}_{1^k3}}{(\alpha^{\mathrm{C}}_1)^k\,\alpha^{\mathrm{C}}_3}$	$\dfrac{\delta^{\mathrm{C}}_{1^k4}}{\left(\delta^{\mathrm{C}}_1\right)^k\delta^{\mathrm{C}}_4}$	$\dfrac{\alpha^{\mathrm{C}}_{1^k4}}{\left(\alpha^{\mathrm{C}}_1\right)^k\alpha^{\mathrm{C}}_4}$
1	0.9170936095	0.96302276	0.811049901	0.909520	0.72767688	0.8651382
2	0.9533118	0.9832182	0.88992782	0.956210	0.83895234	0.9320673
3	0.940068655	0.9745199	0.85954882	0.934729	0.79440126	0.8999692
4	0.94562895	0.978997	0.8725186	0.945638	0.813694	0.916107
5	0.94332356	0.97682	0.866950	0.940206	0.805181	0.907956
6	0.944333	0.97793	0.86948	0.943012	0.80911	0.912162
7	0.94389	0.977368	0.86831	0.941575	0.80722	0.9099954
8	0.94411	0.977671	0.86885	0.94232	0.8078	0.911138
9	0.9439	0.977519	0.8688	0.94193	0.8077	0.910546
10	0.943	0.97761	0.8688	0.94212	0.807	0.91085
11	0.945	0.97765	0.869	0.94205	0.8075	0.91071
12	0.948	0.9776	0.870	0.94211	0.809	0.91083

Table 8 Ratios of the scaling exponents of quintic critical circle maps for the data from Table 6.

	Quintic critical, $\mathsf{T} = (1^k2)$		Quintic critical, $\mathsf{T} = (1^k3)$		Quintic critical, $\mathsf{T} = (1^k4)$	
k	$\dfrac{\delta^{\mathrm{Q}}_{1^k2}}{\left(\delta^{\mathrm{Q}}_1\right)^k\,\delta^{\mathrm{Q}}_2}$	$\dfrac{\alpha^{\mathrm{Q}}_{1^k2}}{\left(\alpha^{\mathrm{Q}}_1\right)^k\,\alpha^{\mathrm{Q}}_2}$	$\dfrac{\delta^{\mathrm{Q}}_{1^k3}}{\left(\delta^{\mathrm{Q}}_1\right)^k\,\delta^{\mathrm{Q}}_3}$	$\dfrac{\alpha^{\mathrm{Q}}_{1^k3}}{\left(\alpha^{\mathrm{Q}}_1\right)^k\,\alpha^{\mathrm{Q}}_3}$	$\dfrac{\delta^{\mathrm{Q}}_{1^k4}}{\left(\delta^{\mathrm{Q}}_1\right)^k\delta^{\mathrm{Q}}_4}$	$\dfrac{\alpha^{\mathrm{Q}}_{1^k4}}{\left(\alpha^{\mathrm{Q}}_1\right)^k\alpha^{\mathrm{Q}}_4}$
1	0.9098198	0.97084	0.7916327	0.929705	0.69812	0.89755
2	0.9509078	0.98652	0.881271	0.96446	0.8227	0.94558
3	0.93539	0.97995	0.84565	0.94907	0.773	0.92375
4	0.94182	0.98283	0.86019	0.95570	0.7918	0.9329
5	0.93926	0.98170	0.85435	0.9531	0.7845	0.92926
6	0.940	0.98206	0.8563	0.9539	0.785	0.9306
7	0.9400	0.98199	0.8559	0.95377	0.786	0.9303
8	0.933	0.9822	0.8537	0.9537	0.7854	0.931
9	0.92	0.9826	0.860	0.9537	0.81	0.9306
10	0.94	0.982	0.87	0.9539	0.82	0.931
11	0.99	0.98	0.9	0.9538	0.8	0.930
12	0.95	0.982	0.9	0.9539	0.7	0.93

was 4 units in the last digit (which, of course, was just an estimate). One should have in mind that the logarithmic scale may give a distorted idea about values very close to zero. Another effect that makes the values for large k less reliable is that their computations involve quite a number of extrapolations. Figure 1 provides an excellent confirmation of the fact that the ratios $\mathcal{D}_k$ and $\mathcal{A}_k$ approach their limiting values exponentially, as claimed by PACSE (cf. (7)), especially if one takes into account that the data represented in the table are very small differences which are extremely sensitive to numerical errors. Note also that the approximate straight lines corresponding to 1^k2, 1^k3, and 1^k4 for medium values of k are

roughly parallel, as predicted. In our opinion it is quite remarkable that one glimpse into the exponential convergence of the ratios of the scaling exponents because in some sense this is a third-order correction. We also think that it is interesting that the asymptotic formula fits so well even for small values of k.

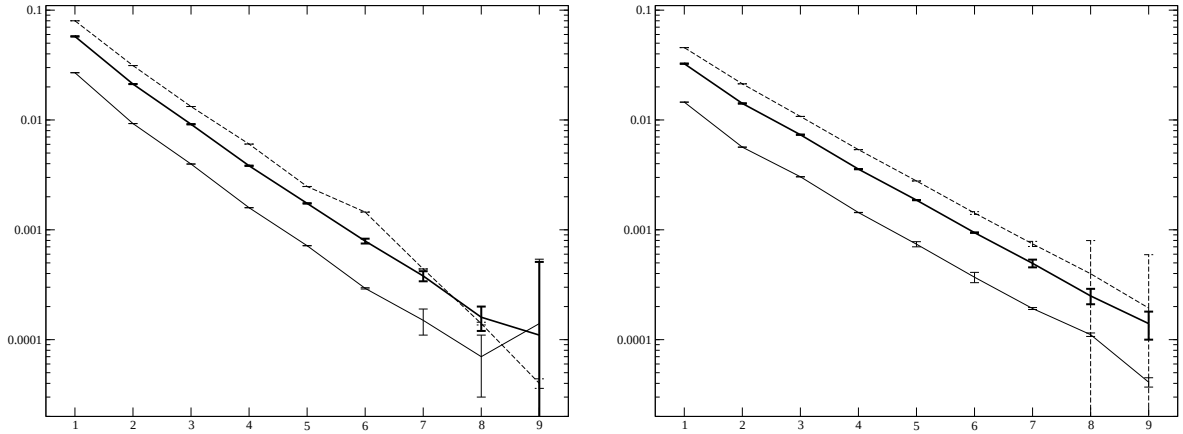

Fig. 1 Left: Log-linear plot of the differences $|\mathcal{D}_k^{\mathrm{C},2} - \mathcal{D}_\infty^{\mathrm{C},2}|$ (thin lines), $|\mathcal{D}_k^{\mathrm{C},3} - \mathcal{D}_\infty^{\mathrm{C},3}|$ (thick lines), $|\mathcal{D}_k^{\mathrm{C},4} - \mathcal{D}_\infty^{\mathrm{C},4}|$ (dashed lines) vs. k for $k = 1, 2, \ldots, 9$; the notations are defined in the text. **Right:** Log-linear plot of the differences $|\mathcal{A}_k^{\mathrm{C},2} - \mathcal{A}_\infty^{\mathrm{C},2}|$ (thin lines), $|\mathcal{A}_k^{\mathrm{C},3} - \mathcal{A}_\infty^{\mathrm{C},3}|$ (thick lines), $|\mathcal{A}_k^{\mathrm{C},4} - \mathcal{A}_\infty^{\mathrm{C},4}|$ (dashed lines) vs. k for $k = 1, 2, \ldots, 9$; the notations are defined in the text.

4.5 Scaling exponents for non-critical circle maps

For critical circle maps one can only compute the scaling exponents numerically, which takes long time (to find each value in Tables 5 and 6 we run the code for weeks) and the accuracy is limited. In the case of non-critical circle maps, however, one can use the fact that the map is conjugate to a rigid rotation (mentioned in Section 4.1) and either write a simple computer code or even do computations by hand. Indeed, the case considered here can be obtained as a particular case of the general results in [35].

Here we will illustrate how one can find the parameter-space scaling exponents for rotation numbers of the form $\langle (1^k m)^\infty \rangle$ for $k \in \mathbb{N}$, $m \geq 2$.

Let $F_0 = 0$, $F_1 = 1$, $F_{n+1} = F_n + F_{n-1}$ ($n \in \mathbb{N}$) be the Fibonacci numbers the ratios of two consecutive ones converge to the golden mean: $\lim\limits_{n\to\infty} \dfrac{F_n}{F_{n+1}} = \langle 1^\infty \rangle$. The general form of F_n is $F_n = C_+(\mu_+)^n + C_-(\mu_-)^n$, where $\mu_\pm = \frac{1}{2}\left(1 \pm \sqrt{5}\right)$ are the roots of the quadratic equation $\mu^2 - \mu - 1 = 0$, and $C_\pm$ are constants; for our choice of initial conditions, they are $C_+ = -C_- = \frac{1}{\sqrt{5}}$. Let $\mathsf{A} = (1^k m)$ and $\omega = \langle \mathsf{A}^\infty \rangle$. Note that $\mathcal{G}^j(\omega) = \langle 1^{k-j} m \mathsf{A}^\infty \rangle$ for $j = 1, \ldots, k$, and $\mathcal{G}^{k+1}(\omega) = \omega$. One easily shows that

$$\langle m\mathsf{A}^\infty \rangle = \frac{1}{m+\omega} \ , \qquad \langle 1^j m \mathsf{A}^\infty \rangle = \frac{F_j(m+\omega) + F_{j-1}}{F_{j+1}(m+\omega) + F_j} \ , \quad j = 1, \ldots, k-1 \ . \tag{15}$$

If one takes $j = k$ in (15), the right-hand side must equal ω. Using this, we solve the equation

$$\omega = \langle 1^k m \mathsf{A}^\infty \rangle = \frac{F_k(m+\omega) + F_{k-1}}{F_{k+1}(m+\omega) + F_k} \ ,$$

to obtain

$$\omega = \frac{1}{2}\left(-m + \sqrt{m^2 + 4\frac{mF_k + F_{k-1}}{F_{k+1}}} \right) \ . \tag{16}$$

To compute the parameter-space scaling exponent δ, we will use the fact that, if a number x is a periodic point under the Gauss map, i.e., $\mathcal{G}^n(x) = x$, then $\delta = (\mathcal{G}^n)'(x)$. This fact is clear because the efect of renormalization on the rotation number is just to apply $\mathcal{G}^n$. Hence, the linearization of this

effect is precisely $(\mathcal{G}^n)'(x)$. Of course, for the family of rigid rotations, the parameter of the family is the rotation number. For a more general family we note that, since $\mathcal{G}^n(x) = x$, x is Diophantine and, by Herman's theorem [29], the map is smoothly conjugate to a rigid rotation. It is well known and not difficult to prove that the rotation number is differentiable as a function of the parameter at this point (the details appear in many places, a reference that also contain algorithms is [39]).

Recalling that $\mathcal{G}'(x) = -\frac{1}{x^2}$ for $x \in (0,1) \setminus \{\frac{1}{2}, \frac{1}{3}, \ldots\}$, we obtain that the derivative of the $(k+1)$st iterate of the Gauss map at ω is equal to

$$\left|\left(\mathcal{G}^{k+1}\right)'(\omega)\right| = \prod_{j=0}^{k} \left|\mathcal{G}'\left(\mathcal{G}^j(\omega)\right)\right| = \prod_{j=0}^{k} \langle 1^j m \mathsf{A}^\infty\rangle^{-2} = \left[F_{k+1}(m+\omega) + F_k\right]^2 \ .$$

Substituting ω from (16), we obtain the non-critical parameter-space scaling exponent for $\langle (1^k m)^\infty\rangle$:

$$\delta^{\mathrm{N}}_{1^k m} = \left|\left(\mathcal{G}^{k+1}\right)'(\omega)\right| = \left[\frac{m}{2}F_{k+1}\left(1 + \sqrt{1 + \frac{4}{m^2}\frac{mF_k + F_{k-1}}{F_{k+1}}}\right) + F_k\right]^2 \ . \tag{17}$$

Using (17) and the fact that $\delta^{\mathrm{N}}_1 = \langle 1^\infty\rangle^{-2} = \mu_+^2$, $\delta^{\mathrm{N}}_m = \langle m^\infty\rangle^{-2} = \frac{1}{2}\left(m + \sqrt{m^2+4}\right)$, we obtain after tedious algebraic manipulations that for large k,

$$\mathcal{D}_k = \frac{\delta^{\mathrm{N}}_{1^k m}}{\left(\delta^{\mathrm{N}}_1\right)^k \delta^{\mathrm{N}}_m} = \left[\frac{2}{\sqrt{5}}\frac{2 + m\mu_+}{m + \sqrt{m^2+4}}\right]^2 + C\mu_+^{-2k} + \cdots =: \mathcal{D}_\infty + C\mu_+^{-2k} + \cdots \ ,$$

where C is a complicated expression depending on the form of the CFE studied but not on k. Therefore, we obtain that the ratios $\mathcal{D}_k$ approach their limiting value $\mathcal{D}_\infty$ exponentially:

$$|\mathcal{D}_k - \mathcal{D}_\infty| \approx C(\mu_+^{-2})^k \ ,$$

– compare this with (7).

This analysis can be easily generalized to rotation numbers of the form $\langle (a^k m)^\infty\rangle$. If $\left\{F_n^{\langle a^\infty\rangle}\right\}_{n=1}^\infty$ is a Fibonacci-like sequence generating $\langle a^\infty\rangle$, then

$$F_n^{\langle a^\infty\rangle} = C_+\left(\mu_+^{\langle a^\infty\rangle}\right)^n + C_-\left(\mu_-^{\langle a^\infty\rangle}\right)^n \ ,$$

where

$$\mu_\pm^{\langle a^\infty\rangle} = \frac{1}{2}\left(a \pm \sqrt{a^2+4}\right)$$

are the roots of the quadratic equation $\mu^2 - a\mu - 1 = 0$, and C_+ and C_- are constants that do not depend on n. In this case the approach of $\mathcal{D}_k$ to its limit is given by

$$\mathcal{D}_k = \mathcal{D}_\infty + C\left(\mu_+^{\langle a^\infty\rangle}\right)^{-2k} + \cdots \ .$$

If ξ^{N}_a is the constant in (7) that characterizes the rate at which the ratios $\mathcal{D}_k$ approach their limiting value $\mathcal{D}_\infty$, then

$$\xi^{\mathrm{N}}_a = \left(\mu_+^{\langle a^\infty\rangle}\right)^{-2} = \left(\frac{a + \sqrt{a^2+4}}{2}\right)^{-2} = \frac{a^2 + 2 - \sqrt{a^2+4}}{2} \ . \tag{18}$$

In Figure 2 we present numerical data for $|\mathcal{D}_k - \mathcal{D}_\infty|$ vs. k in the non-critical case, for several rotation numbers. To obtain these values, we used that a non-critical map with an eventually periodic rotation number is smoothly conjugate to a rigid rotation, which allowed us to compute the numerical values of the scaling exponents quickly and with arbitrarily high accuracy. We computed the parameter-space scaling exponents for rotation numbers $\langle (1^k 2)^\infty\rangle$, $\langle (1^k 7)^\infty\rangle$, and $\langle (1^k 22)^\infty\rangle$ (drawn with straight lines in Figure 2), as well as for $\langle (3^k 2)^\infty\rangle$ and $\langle (3^k 7)^\infty\rangle$ (drawn with straight lines in Figure 2). We measured the slopes of the straight lines in the figure and found them to be approximately -0.417975 for the cases $\langle (1^k \mathsf{B})^\infty\rangle$ and -1.037758 for the cases $\langle (3^k \mathsf{B})^\infty\rangle$. These values are in excellent agreement with the theoretical predictions for the slopes which, according to (18), should be $\log_{10}\xi^{\mathrm{N}}_1 = \log_{10}\frac{3-\sqrt{5}}{2}$ and $\log_{10}\xi^{\mathrm{N}}_3 = \log_{10}\frac{11-3\sqrt{13}}{2}$. In the figure we also plotted the data for $\langle (1^k 22)^\infty\rangle$ to show that the slope in this case is the same as for $\langle (1^k 2)^\infty\rangle$ and $\langle (1^k 7)^\infty\rangle$.

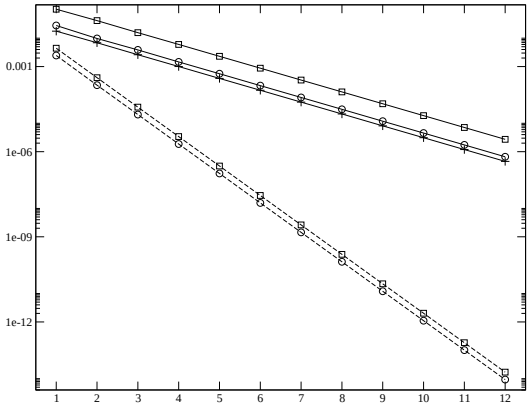

Fig. 2 Log-linear plot of $|\mathcal{D}_k - \mathcal{D}_\infty|$ vs. k for non-critical circle maps with rotation numbers $\langle(1^k2)^\infty\rangle$ (circles and solid line), $\langle(1^k7)^\infty\rangle$ (squares and solid line), $\langle(3^k2)^\infty\rangle$ (circles and dashed line), $\langle(3^k7)^\infty\rangle$ (squares and dashed line), $\langle(1^k22)^\infty\rangle$ (pluses and solid line).

5 PACSE for dynamics on boundaries of Siegel disks

5.1 Preliminaries

Let f be a holomorphic map of the complex plane $\mathbb{C}$ of the form

$$f(z) = \mathrm{e}^{2\pi i\sigma} z + \mathcal{O}(z^2) \; ; \tag{19}$$

$\sigma \in [0,1)$ is called the *rotation number* of f. By a theorem of Siegel [53](see also [30, Sec. 2.8]), if σ satisfies some Diophantine conditions, then there exists a unique analytic map h, called *conjugacy*, from an open disk $B(0,r)$ around the origin to $\mathbb{C}$ such that $h(0) = 0$, $h'(0) = 1$, and $f \circ h(z) = h(\mathrm{e}^{2\pi i\sigma} z)$. We will be interested only in eventually periodic rotation numbers, in which case the Diophantine conditions are satisfied.

Let R_S be the radius of the largest open disk for around the origin, $B(0, R_\mathrm{S})$, for which the conjugacy h exists; R_S is called the *Siegel radius*. The *Siegel disk*, $\mathcal{D}_\mathrm{S}$, is the image of $B(0, R_\mathrm{S})$ under h: $\mathcal{D}_\mathrm{S} = h(B(0, R_\mathrm{S}))$. For $r < R_\mathrm{S}$, the image of $\partial B(0,r) = \{w \in \mathbb{C} : |w| = r\}$ under h is an analytic circle. The dynamics of a point z with $|z| = r < R_\mathrm{S}$ is very simple: the identity $f^n \circ h(z) = h(\mathrm{e}^{2\pi i\sigma n} z)$ guarantees that the iterates $f^n(z)$ fill the analytic circle $h(\partial B(0,r))$ densely with a smooth density (since the points $\{\mathrm{e}^{2\pi i\sigma n} z\}_{n\in\mathbb{N}}$ fill $\partial B(0,r)$ uniformly).

The boundary $\partial\mathcal{D}_\mathrm{S}$ of the Siegel disk, however, is not a smooth curve. It was discovered numerically in [42] that the dynamics of the map f on $\partial\mathcal{D}_\mathrm{S}$ exhibits interesting scaling properties. Soon after this observation, [64] suggested a renormalization-group explanation. The renormalization-group theory was later developed in [60,59] and, more recently, in [24,25], among others. Recently, two of the authors of the present paper studied some regularity properties of h on the boundary [38].

5.2 PACSE for the dynamics of iterates on $\partial\mathcal{D}_\mathrm{S}$

In this section we define scaling exponents governing the dynamics of iterates on $\partial\mathcal{D}_\mathrm{S}$, and give numerical data in support of PACSE in this case. We will be interested only in eventually periodic rotation numbers, $\sigma = \langle\mathsf{HT}^\infty\rangle$, in which case a theorem from [27] guarantees that $\partial\mathcal{D}_\mathrm{S}$ contains a critical point c of f. We study maps with only one critical point $c \in \partial\mathcal{D}_\mathrm{S}$. We define the *order of criticality* d as the multiplicity of the critical point c: $f^{(k)}(c) = 0$ for $k = 1, 2, \ldots, d$, and $f^{(d+1)}(c) \neq 0$.

We studied only the the configuration-space scaling exponent which is defined as follows. Let f be a holomorphic map of $\mathbb{C}$ of the form (19) with rotation number $\langle\mathsf{HT}^\infty\rangle$, the point c be the only critical point of f in $\partial\mathcal{D}_\mathrm{S}$, and $\frac{P_n}{Q_n} = \langle\mathsf{HT}^n\rangle$ be rational approximants to $\langle\mathsf{HT}^\infty\rangle$, then the configuration-space scaling exponent α_T is defined by

$$\alpha_\mathsf{T}^{-1} = \lim_{n\to\infty} \left| \frac{f^{Q_{n+1}}(c) - c}{f^{Q_n}(c) - c} \right| \; . \tag{20}$$

We emphasize that, according to our definition, α_{T} is a real number. Since in the Siegel disk case it is not easy to change parameters, we do not consider the parameter-space scaling exponents.

The formulation of PACSE in this case is identical to that for circle maps (see Sections 2.2 and 4.4).

We studied the following family of maps:

$$f_{m,\sigma,\zeta}(z) = \frac{1}{\zeta} \mathrm{e}^{2\pi i\sigma} \left[g_{m+1}(z) - (1-\zeta) g_m(z) \right] \ , \tag{21}$$

where $m \in \mathbb{N}$, $\zeta \in \mathbb{C}$, and the function $g_m : \mathbb{C} \to \mathbb{C}$ is defined as

$$g_m(z) = \frac{1}{m+1} \left[1 - (1-z)^{m+1} \right] \ .$$

For the map (21),

$$f'_{m,\sigma,\zeta}(z) = \mathrm{e}^{2\pi i\sigma} (1-z)^m \left(1 - \frac{z}{\zeta} \right) \ ,$$

so that $f_{m,\sigma,\zeta}(0) = 0$, $f'_{m,\sigma,\zeta}(0) = \mathrm{e}^{2\pi i\sigma}$. If ζ is large enough so that it is outside the closure of the Siegel disk, then the point $c = 1$ is the only critical point in $\partial\mathcal{D}_{\mathrm{S}}$. In this case the order of criticality of c is $d = m$. If $\zeta = 1$, then $d = m + 1$.

We computed the scaling exponents $\alpha_{\mathsf{T}}^{(d)}$ for orders of criticality $d = 1$ and $d = 2$ for rotation numbers of the form $\langle \mathsf{T}^{\infty} \rangle$ for $\mathsf{T} = (1^k 2)$, $\mathsf{T} = (1^k 3)$, and $\mathsf{T} = (1^k 4)$. The results of our computations are collected in Table 9, and their ratios are given in Table 10.

Table 9 Configuration-space scaling exponents $\alpha_{\mathsf{T}}^{(d)}$ (20) for dynamics on $\partial\mathcal{D}_{\mathrm{S}}$ for orders of criticality $d = 1$ and $d = 2$ and rotation numbers $\langle \mathsf{T}^{\infty} \rangle$, with $\mathsf{T} = (1^k 2)$, $(1^k 3)$, and $(1^k 4)$.

	Order of criticality $d = 1$			Order of criticality $d = 2$		
k	$\alpha^{(1)}_{1^k 2}$	$\alpha^{(1)}_{1^k 3}$	$\alpha^{(1)}_{1^k 4}$	$\alpha^{(2)}_{1^k 2}$	$\alpha^{(2)}_{1^k 3}$	$\alpha^{(2)}_{1^k 4}$
0	1.7208355451952	2.0638087530123	2.354977763868	1.4576963100	1.64668352299	1.7913966317
1	2.22549030564756	2.5112478301746996	2.721163460566	1.7361660641	1.869697973	1.957675854
2	3.06380245567	3.55743499210	3.94372251939	2.17513015	2.39443077	2.54730947
3	4.0942962273	4.69458675007	5.14895784724	2.659144280	2.8983004	3.05945269
4	5.5404202266	6.38899852	7.0402706951	3.2845585	3.5949893	3.80691370
5	7.4542574779	8.57315493	9.425443522	4.038873 ± 0.000003	4.412764	4.666404
6	10.055427659	11.578952	12.743216	4.975503 ± 0.000005	5.439646	5.755377
7	13.54775	15.5911804	17.14996481	6.12528 ± 0.00001	6.6955 ± 0.0001	7.08306
8	18.2634765	21.024061	23.1315797	7.54226	8.2443 ± 0.0001	8.72188
9	24.61390	28.33045	31.1665389	9.28679	10.152	10.740
10	33.1769	38.18889	42.014	11.434	12.50 ± 0.01	13.223
11	44.715	51.469	56.623	14.079	15.39	16.283
12	60.270	69.37 ± 0.01	76.322	17.335 ± 0.005	18.95 ± 0.01	20.048
13	81.233	93.503	102.86	21.345 ± 0.005	23.334 ± 0.004	24.686

The values of the configuration-space scaling exponents for dynamics on $\partial\mathcal{D}_{\mathrm{S}}$ (Table 9) can be computed numerically with good accuracy. The fact that the values of $\mathcal{A}_k$ approach $\mathcal{A}_\infty$ exponentially – which is the content of part (c) of PACSE expressed in equation (7) – can be seen very clearly in Figure 3. If $\mathcal{A}_k^{(d),m} = \frac{\alpha^{(d)}_{1^k m}}{(\alpha_1^{(d)})^k \alpha_m^{(d)}}$ and $\mathcal{A}_\infty^{(d),m}$ be the limiting value of $\mathcal{A}_k^{(d),m}$ as $k \to \infty$, then the values we used to plot Figure 3 are $\mathcal{A}_\infty^{(1),2} = 0.974388$, $\mathcal{A}_\infty^{(1),3} = 0.935178$, $\mathcal{A}_\infty^{(1),4} = 0.901625$, $\mathcal{A}_\infty^{(2),2} = 0.97939$, $\mathcal{A}_\infty^{(2),3} = 0.94778$, and $\mathcal{A}_\infty^{(2),4} = 0.92166$ (we found them by Aitken extrapolation from the corresponding values in Table 10). The error bars were plotted under the assumption that the error was 4 units in the last digit displayed in Table 10. Again, although the values represented graphically in Figure 3 are extremely sensitive to numerical errors, the exponential convergence of $\mathcal{A}_k$ to its limit (part (c) of PACSE) is clear from the figure.

From the data presented in Table 10 we could even extract quite accurately the values of the constants $\eta_{\mathsf{A}}^{(d)}$ characterizing the rate at which the ratios $\mathcal{A}_k$ approach their limits; we define these constants as in (7):

$$\left| \frac{\alpha^{(d)}_{\mathsf{A}^k\mathsf{B}}}{\left(\alpha_{\mathsf{A}}^{(d)}\right)^k \alpha_{\mathsf{B}}^{(d)}} - \lim_{j\to\infty} \frac{\alpha^{(d)}_{\mathsf{A}^j\mathsf{B}}}{\left(\alpha_{\mathsf{A}}^{(d)}\right)^j \alpha_{\mathsf{B}}^{(d)}} \right| \approx C_{\mathsf{A},\mathsf{B},d} \left(\eta_{\mathsf{A}}^{(d)}\right)^k \ ,$$

Table 10 Ratios of the α's for the data from Table 9.

	Order of criticality $d=1$			Order of criticality $d=2$		
k	$\dfrac{\alpha^{(1)}_{1^k2}}{\left(\alpha^{(1)}_1\right)^k\alpha^{(1)}_2}$	$\dfrac{\alpha^{(1)}_{1^k3}}{\left(\alpha^{(1)}_1\right)^k\alpha^{(1)}_3}$	$\dfrac{\alpha^{(1)}_{1^k4}}{\left(\alpha^{(1)}_1\right)^k\alpha^{(1)}_4}$	$\dfrac{\alpha^{(2)}_{1^k2}}{\left(\alpha^{(2)}_1\right)^k\alpha^{(2)}_2}$	$\dfrac{\alpha^{(2)}_{1^k3}}{\left(\alpha^{(2)}_1\right)^k\alpha^{(2)}_3}$	$\dfrac{\alpha^{(2)}_{1^k4}}{\left(\alpha^{(2)}_1\right)^k\alpha^{(2)}_4}$
1	0.959512368101934	0.902785059057004	0.8572984892172	0.96730802917	0.9221507023	0.8875434331
2	0.980053691355	0.948846586560	0.921824011949	0.984236263	0.959120808	0.937931507
3	0.97170090800	0.929010524787	0.892946092480	0.9772295695	0.94287693	0.914900238
4	0.97557416743	0.938037696	0.90585670054	0.98032998	0.94983856	0.924578126
5	0.97383687199	0.933882881	0.8997796718	0.9790301	0.9468986	0.9204358
6	0.97464533584	0.93580473	0.90256329	0.9795203	0.9479905	0.9219885
7	0.974262	0.934887205	0.9012101866	0.979361	0.94767	0.921538
8	0.974446477	0.93532182	0.901846013	0.979398	0.94769	0.921601
9	0.9743595	0.9351089	0.901529436	0.97941	0.94778	0.92172
10	0.974403	0.93521184	0.90167	0.97935	0.9478	0.92160
11	0.97436	0.93515	0.90160	0.97938	0.9477	0.92170
12	0.97439	0.9351	0.90164	0.97936	0.9477	0.92165
13	0.97438	0.93517	0.90156	0.97939	0.94778	0.92169

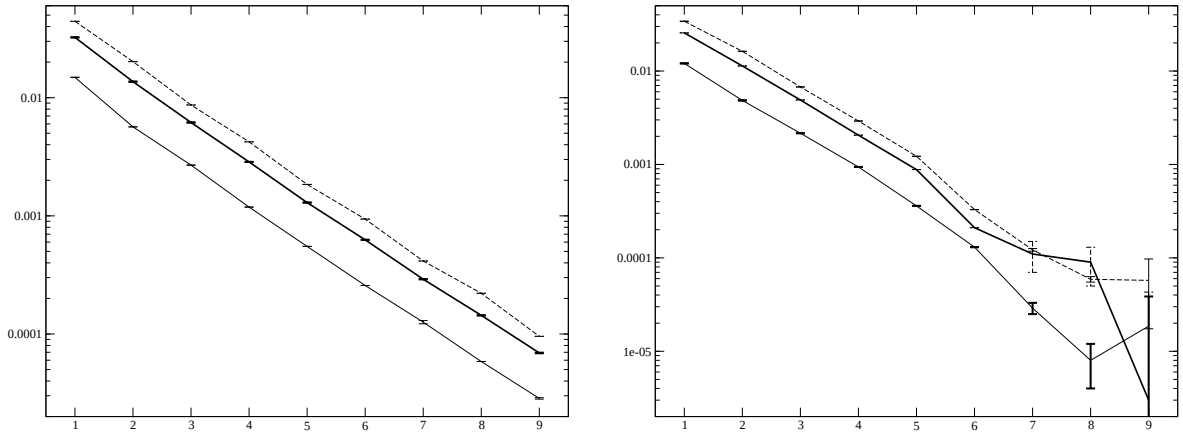

Fig. 3 Log-linear plots of $\left|\mathcal{A}_k^{(d),m}-\mathcal{A}_\infty^{(d),m}\right|$ vs. k for maps of Siegel disk with orders of criticality $d=1$ (left) and $d=2$ (right) with rotation numbers $\langle(1^k2)^\infty\rangle$ (thin solid lines), $\langle(1^k3)^\infty\rangle$ (thick lines), $\langle(1^k4)^\infty\rangle$ (dashed lines); see the text for the notations and the values of $\mathcal{A}_\infty^{(d),m}$ for the different cases.

or, in the short notations introduced above (for $\mathsf{A}=1$, $\mathsf{B}=m=2,3,4$, $d=1,2$),

$$|\mathcal{A}_k^{(d),m}-\mathcal{A}_\infty^{(d),m}|\approx C_{1,m,d}\left(\eta_1^{(d)}\right)^k\ .$$

We performed an exponential regression on the data from Table 10 for $k=2$, 3, 4, and 5, where, as one can see from Figure 3, the exponential convergence has already developed but the data are still not contaminated by numerical errors. From each line in the plots from Figure 3 we found the value of the corresponding $\eta_1^{(d)}$, and obtained the following numerical values:

$$\eta_1^{(1)}=\begin{cases}0.458\pm0.005 & \text{for } m=2 \text{ (left plot, thin solid line)}\ ,\\ 0.457\pm0.002 & \text{for } m=3 \text{ (left plot, thick line)}\ ,\\ 0.454\pm0.008 & \text{for } m=4 \text{ (left plot, dashed line)}\ ;\end{cases}$$

$$\eta_1^{(2)}=\begin{cases}0.422\pm0.011 & \text{for } m=2 \text{ (right plot, thin solid line)}\ ,\\ 0.426\pm0.002 & \text{for } m=3 \text{ (right plot, thick line)}\ ,\\ 0.423\pm0.002 & \text{for } m=4 \text{ (right plot, dashed line)}\ .\end{cases}$$

There is an excellent agreement among the three values for each $\eta_1^{(d)}$ that were obtained from different m. Furthermore, the numerical data for $\eta_1^{(d)}$ and $\eta_1^{(2)}$ differ by a comfortable margin, which makes it clear that the rate of convergence depends on the order of criticality d of the critical point of the map.

6 PACSE for area-preserving twist maps

6.1 Preliminaries

Let $f : \mathbb{T} \times \mathbb{R} \to \mathbb{T} \times \mathbb{R}$ be an *area-preserving twist map* (APTM), i.e., a C^1 diffeomorphism from the cylinder to itself that preserves area, orientation, and the topological ends of $\mathbb{T} \times \mathbb{R}$, and satisfies the twist condition,

$$\frac{\partial \overline{x}}{\partial y} > 0 \ , \qquad \text{where} \qquad (\overline{x}, \overline{y}) = f(x, y) \ .$$

Let F stand for the *lift* of f to $\mathbb{R}^2$, the universal cover of the cylinder. We will consider a "standard-like" one-parameter family f_μ of APTMs,

$$\overline{x} = x + \overline{y} \ , \qquad \overline{y} = y + g(x) \ ,$$

where g is a periodic function of period 1. We also assume that $\int_0^1 g(x)\,\mathrm{d}x = 0$ (the *zero flux condition*), which guarantees that the oriented area between any non-contractible circle and its image under f is zero. In our numerical simulations we used the so-called *standard* (or *Chirikov-Taylor*) *map*, $\{f_\mu\}_\mu$,

$$\overline{x} = x + \overline{y} \ , \qquad \overline{y} = y + \frac{\mu}{2\pi} \sin x \ . \tag{22}$$

The *rotation number*, $\tau(x, y)$, of the orbit $\{f^n(x, y)\}_{n=0}^{\infty}$ of (x, y) is defined as $\lim_{n\to\infty} \frac{1}{n} \pi_1[F^n(x, y) - x]$, where $\pi_1 : \mathbb{R}^2 \to \mathbb{R}$ is the projection onto the first coordinate. In contrast with the case of circle maps, this limit may not exist, and it depends on the point (x, y). A periodic orbit of f of period q has rotation number $\frac{p}{q}$ (with $p, q \in \mathbb{N}$) if $F^q(x, y) = (x, y) + (p, 0)$.

Any topologically nontrivial invariant circle of f is the graph of a Lipschitz function [43]. For any Diophantine rotation number ρ, there exists a critical value μ_ρ such that for $\mu < \mu_\rho$ there exists a topologically nontrivial invariant circle of rotation number ρ, while for $\mu > \mu_\rho$ such circle does not exist. In early 1980's, a renormalization group description of the dynamics of the APTM in a neighborhood of the critical value μ_ρ has been developed in [40,41]; a mathematical discussion of this description can be found in [58,61]. The scaling properties are related also to the regularities of certain functions associated with the invariant circles, as shown in [47].

The renormalization group description is based on certain assumptions. The renormalization operator has an attractive fixed point (trivial) and a hyperbolic (non-trivial) fixed point. The hyperbolic fixed point has only one unstable direction.

The *obstruction criterion* [48,49] is a method to determine the non-existence of invariant circles for a one parameter family of APTM. This criterion is consistent with the renormalization group assumptions, as shown in [34]. The obstruction criterion can be formulated briefly as follows. Assume that f has hyperbolic periodic points z_n and $z_{n'}$ of rotation numbers $\frac{p_n}{q_n}$ and $\frac{p_{n'}}{q_{n'}}$, respectively, with $\frac{p_n}{q_n} < \rho < \frac{p_{n'}}{q_{n'}}$. Assume, moreover, that the stable manifold of z_n intersects the unstable manifold of $z_{n'}$. Then, there is no homotopically non-trivial invariant circle with a rotation number $\rho \in [\frac{p_n}{q_n}, \frac{p_{n'}}{q_{n'}}]$, as shown in [48,49].

The obstruction criterion allows us to define a codimension-one bifurcation manifold (in an appropriately defined function space of APTMs) which has a transversal intersection with the unstable manifold of the nontrivial point of the renormalization operator $\mathcal{R}_\rho$ [34]. The bifurcation manifold is defined as the set of maps such that the local stable manifold $W^{\mathrm{s}}_{z_n}$ of z_n has exactly one point of tangency with the local unstable invariant manifold $W^{\mathrm{u}}_{z_{n'}}$ of $z_{n'}$. Let the rotation numbers $\frac{p_n}{q_n}$ and $\frac{p_{n'}}{q_{n'}}$ be two consecutive rational approximants of the Diophantine rotation number ρ and $\frac{p_n}{q_n} < \rho < \frac{p_{n'}}{q_{n'}}$. When the local invariant manifolds $W^{\mathrm{s}}_{z_n}$ and $W^{\mathrm{u}}_{z_{n'}}$ has two transversal intersection, we can define a lobe which is enclosed by the two segments of $W^{\mathrm{s}}_{p_n}$ and $W^{\mathrm{u}}_{p_{n'}}$ bounded by the two heteroclinic intersection points, as shown in Figures 2 and 4 of [34]. In this way we can define a foliation of codimension-one surfaces of APTMs for which the area of the lobe is exactly A_n. These surfaces approach the bifurcation manifold when the area of the lobe goes to zero.

6.2 Scaling exponents and PACSE for APTMs

Here we will define the scaling exponents on the example of the one-parameter family (22), following [34]. There the authors define a foliation of codimension-one manifolds $\{\Lambda_{n,\gamma}\}_{n\in\mathbb{N}}$ in the function space as

Table 11 Scaling exponets for the standard map (22) with rotation numbers $\langle \mathsf{T}^\infty \rangle$, $\mathsf{T} = (21^k)$, (31^k), and (32^k).

k	δ_{21^k}	α_{21^k}	δ_{31^k}	α_{31^k}	δ_{32^k}	α_{32^k}
0	2.44159	14.60	3.34437	40.12	3.34437	40.12
1	3.77840	59.54	4.79135	146.93	8.03772	591.54
2	6.29843	284.53	8.27110	652.71	19.7013	10197
3	10.1680	1,141.4	13.1775	2,909.7	47.6478	13,523
4	16.6101	4,935.4	21.5442	11,623	111.980	1,649,000
5	27.0411	21,356	34.6905	54,284	301.401	34,543,000
6	43.9826	94,282	62.3650	214,010	?	?

Table 12 Ratios of the scaling exponents from Table 11.

k	$\frac{\delta_{21^k}}{\delta_2\,(\delta_1)^k}$	$\frac{\alpha_{21^k}}{\alpha_2\,(\alpha_1)^k}$	$\frac{\delta_{31^k}}{\delta_3\,(\delta_1)^k}$	$\frac{\alpha_{31^k}}{\alpha_3\,(\alpha_1)^k}$	$\frac{\delta_{32^k}}{\delta_3\,(\delta_2)^k}$	$\frac{\alpha_{32^k}}{\alpha_3\,(\alpha_2)^k}$
1	0.950553	0.9398	0.880003	0.8440	0.984344	1.0099
2	0.973287	1.0351	0.933103	0.8641	0.988183	1.1924
3	0.965125	0.9569	0.913146	0.8877	0.978844	1.0830
4	0.968416	0.9536	0.917016	0.8172	0.942187	0.9046
5	0.968397	0.9509	0.906980	0.8796	1.038653	1.2979
6	0.967499	0.9675	1.001540	0.7992	?	?

follows. Let $\left\{\frac{p_n}{q_n}\right\}_{n\in\mathbb{N}}$ be a sequence of rational approximants to the quadratic irrational $\langle \mathsf{T}^\infty \rangle$, $\frac{p_n}{q_n} = \langle \mathsf{T}^n \rangle$. Consider a periodic orbit of rotation number $\frac{p_n}{q_n}$, and let τ_n be the highest eigenvalue of Df^{q_n} along this periodic orbit. Choose some constant γ. Let the foliation $\{\Lambda_{n,\gamma}\}_{n\in\mathbb{N}}$ be defined by the condition $\frac{\tau_n}{\tau_{n+1}} = \gamma$. For the one-parameter family (22), let μ_n be the value of the parameter μ for which $f_{\mu_n} \in \Lambda_{n,\gamma}$, and let A_n be the corresponding lobe area.

The parameter values μ_n converge exponentially to a limit μ_∞, at a rate given by the *parameter-space* scaling exponent δ_T, i.e., $\mu_n \approx \mu_\infty + a\delta_\mathsf{T}^{-n}$ for some constant a (cf. (1)). The *configuration-space* scaling exponent α_T is defined through the ratios of two consecutive lobe areas: $\alpha_\mathsf{T}^{-1} = \lim_{n\to\infty} \dfrac{A_{n+1}}{A_n}$ (cf. (3)). For details about the definitions and a description of the sophisticated numerical methods used in the computations we refer the reader to the paper [34].

The formulation of PACSE for twist maps is similar to that for circle maps given in Section 4.4. The $\star$ operation among rotation numbers is defined as concatenation as in (12). We computed the scaling exponents for rotation numbers of the form $\langle \mathsf{T}^\infty \rangle$ for T equal to (21^k), (31^k), and (32^k). Note that the exponent for $\mathsf{T} = (21^k)$ is the same as for $\mathsf{T} = (1^k 2)$ because the tail of a CFE is defined up to a cyclic permutation. In the computations we used about 30 decimal digits of accuracy provided by the software package DOUBLEDOUBLE [5].

The values of the scaling exponents for APTMs are shown in Table 11, and the ratios $\mathcal{D}_k$ and $\mathcal{A}_k$ (6) are collected in Table 12. In the computations of the ratios (Table 12), we needed the values of α_1 and δ_1, which we computed to be $\alpha_1 = 4.33916$ and $\delta_1 = 1.62802$. Since the computations of the scaling exponents for APTMs is a result of a complicated multi-step procedure, it is impossible to even roughly estimate the errors in the computations. Only in the case of the rotation numbers of the form $\langle (21^k)^\infty \rangle$ the convergence of the ratios $\mathcal{D}_k$ and $\mathcal{A}_k$ to limits can clearly be seen from the values in Table 12, but the fact that the ratios of such large numbers are so close speaks for itself.

7 Proposed renormalization-group interpretation of PACSE

Obtaining the numerical values of the scaling exponents, albeit interesting and challenging, was not our primary goal. Our main interest is in interpreting these numerical results as consequences of some theorems about the global behavior of the renormalization operators. We believe that PACSE indicates that there exist global renormalization group descriptions for maps of all rotation numbers (or all kneading sequences), and that it is possible that PACSE is an evidence for certain dynamical behavior of these renormalization operators, i.e., the existence of a horseshoe with a one-dimensional unstable manifold which, furthermore, satisfies some transversality conditions. We study these questions rigorously in a companion paper [35], and here only give a brief sketch of our ideas.

Let $\mathscr{S}$ stand for an appropriately chosen Banach space of functions, let A and B be finite symbolic sequences, and $\mathscr{D}_{\mathsf{A}} \subset \mathscr{S}$ and $\mathscr{D}_{\mathsf{B}} \subset \mathscr{S}$ be disjoint sets in $\mathscr{S}$. Let $\mathcal{R}_{\mathsf{A}} : \mathscr{D}_{\mathsf{A}} \to \mathscr{S}$ and $\mathcal{R}_{\mathsf{B}} : \mathscr{D}_{\mathsf{B}} \to \mathscr{S}$ be renormalization operators corresponding to A and B, respectively. Define the renormalization operator $\mathcal{R} : \mathscr{D}_{\mathsf{A}} \cup \mathscr{D}_{\mathsf{B}} \to \mathscr{S}$ by

$$\mathcal{R}(f) = \begin{cases} \mathcal{R}_{\mathsf{A}}(f) & \text{if } f \in \mathscr{D}_{\mathsf{A}} \ , \\ \mathcal{R}_{\mathsf{B}}(f) & \text{if } f \in \mathscr{D}_{\mathsf{B}} \ . \end{cases} \tag{23}$$

Let $f_{\mathsf{A}} \in \mathscr{D}_{\mathsf{A}}$ and $f_{\mathsf{B}} \in \mathscr{D}_{\mathsf{B}}$ (represented by full circles in Figure 4) be fixed points of the renormalization operator:

$$\mathcal{R}(f_{\mathsf{A}}) = f_{\mathsf{A}} \ , \qquad \mathcal{R}(f_{\mathsf{B}}) = f_{\mathsf{B}} \ .$$

Assume that the fixed points f_{A} and f_{B} are hyperbolic, with one-dimensional unstable manifolds $W^{\mathrm{u}}_{\mathsf{A}}$ and $W^{\mathrm{u}}_{\mathsf{B}}$, and codimension-one stable manifolds $W^{\mathrm{s}}_{\mathsf{A}}$ and $W^{\mathrm{s}}_{\mathsf{B}}$, respectively. We assume that $W^{\mathrm{u}}_{\mathsf{A}}$ intersects transversely $W^{\mathrm{s}}_{\mathsf{B}}$, and that $W^{\mathrm{u}}_{\mathsf{B}}$ intersects transversely $W^{\mathrm{s}}_{\mathsf{A}}$, as shown in Figure 4. Let $h_{\mathsf{A}} = W^{\mathrm{s}}_{\mathsf{A}} \cap W^{\mathrm{u}}_{\mathsf{B}}$ and

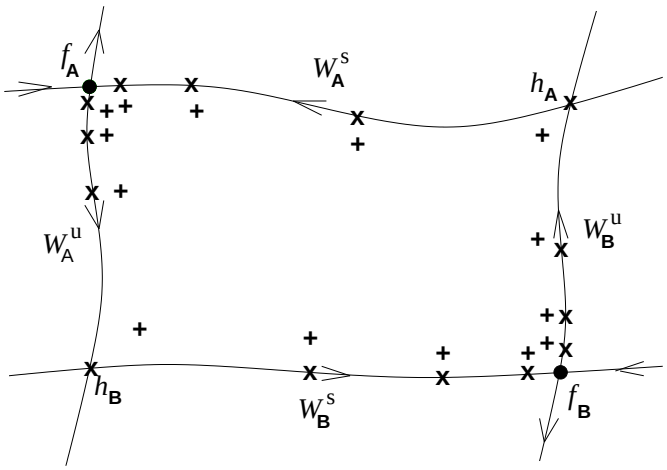

Fig. 4 A schematic representation of the explanation of PACSE.

$h_{\mathsf{B}} = W^{\mathrm{u}}_{\mathsf{A}} \cap W^{\mathrm{s}}_{\mathsf{B}}$ be the intersection points. The transversality of the intersection of the manifolds can be expressed as

$$\mathscr{S} = T_{h_{\mathsf{A}}} W^{\mathrm{s}}_{\mathsf{A}} \oplus T_{h_{\mathsf{A}}} W^{\mathrm{u}}_{\mathsf{B}} \ , \qquad \mathscr{S} = T_{h_{\mathsf{B}}} W^{\mathrm{u}}_{\mathsf{A}} \oplus T_{h_{\mathsf{B}}} W^{\mathrm{s}}_{\mathsf{B}} \ .$$

The scaling exponents for a given symbolic sequence are related to the properties of the renormalization operators corresponding to this symbolic sequence. We will briefly outline how PACSE follows from the assumptions stated above about the geometric properties of the stable and unstable manifolds of the renormalization operators $\mathcal{R}_{\mathsf{A}}$ and $\mathcal{R}_{\mathsf{B}}$.

Let k and m be large enough positive integers, and let $\mathcal{R}_{\mathsf{A}^{\star k} \star \mathsf{B}^{\star m}}$ be the renormalization operator corresponding to the combined symbolic sequence $\mathsf{A}^{\star k} \star \mathsf{B}^{\star m}$. We will give an explicit construction of a fixed point $f_{\mathsf{A}^{\star k} \star \mathsf{B}^{\star m}}$ of $\mathcal{R}_{\mathsf{A}^{\star k} \star \mathsf{B}^{\star m}}$. Let

$$k = k' + k'' + 1 \ , \qquad m = m' + m'' + 1 \ ,$$

where k', k'', m' and m'' are non-negative integers such that $k' \approx k''$ and $m' \approx m''$ (clearly, there is arbitrariness in the choice of k', k'', m' and m'', but it will not affect our conclusions). Consider the following sequence of $(k+m)$ points in $\mathscr{S}$:

$$\begin{aligned} \widetilde{\mathcal{O}}_{\mathsf{A}^{\star k}, \mathsf{B}^{\star m}} := \Big(\quad & h_{\mathsf{A}}, \ \mathcal{R}_{\mathsf{A}}(h_{\mathsf{A}}), \ \mathcal{R}^2_{\mathsf{A}}(h_{\mathsf{A}}), \ \ldots, \ \mathcal{R}^{k'}_{\mathsf{A}}(h_{\mathsf{A}}), \ \mathcal{R}^{-k''}_{\mathsf{A}}(h_{\mathsf{B}}), \ \mathcal{R}^{-k''+1}_{\mathsf{A}}(h_{\mathsf{B}}), \ \ldots, \ \mathcal{R}^{-1}_{\mathsf{A}}(h_{\mathsf{B}}), \\ & h_{\mathsf{B}}, \ \mathcal{R}_{\mathsf{B}}(h_{\mathsf{B}}), \ \mathcal{R}^2_{\mathsf{B}}(h_{\mathsf{B}}), \ \ldots, \ \mathcal{R}^{m''}_{\mathsf{B}}(h_{\mathsf{B}}), \ \mathcal{R}^{-m'}_{\mathsf{B}}(h_{\mathsf{A}}), \ \mathcal{R}^{-m'+1}_{\mathsf{B}}(h_{\mathsf{A}}), \ \ldots, \ \mathcal{R}^{-1}_{\mathsf{B}}(h_{\mathsf{A}}) \ \Big) \end{aligned}$$

(where $\mathcal{R}^n_{\mathsf{A}}$ stands for the n-fold composition of the operator $\mathcal{R}_{\mathsf{A}}$). In Figure 4 these points are represented by the symbol $\times$. Note that the backward iterates of $\mathcal{R}_{\mathsf{A}}$ and $\mathcal{R}_{\mathsf{B}}$ are well-defined. Let $\widetilde{\mathcal{O}}_{(\mathsf{A}^{\star k}, \mathsf{B}^{\star m})^{\star \infty}}$ stand for an infinite sequence of points obtained by repeating infinitely many times the sequence $\widetilde{\mathcal{O}}_{\mathsf{A}^{\star k}, \mathsf{B}^{\star m}}$.

The sequence of points $\left(h_{\mathsf{A}}, \mathcal{R}_{\mathsf{A}}(h_{\mathsf{A}}), \ldots, \mathcal{R}_{\mathsf{A}}^{k'}(h_{\mathsf{A}}), \mathcal{R}_{\mathsf{A}}^{-k''}(h_{\mathsf{B}}), \ldots, \mathcal{R}_{\mathsf{A}}^{-1}(h_{\mathsf{B}}), h_{\mathsf{B}}\right)$ is a pseudoorbit of the operator $\mathcal{R}_{\mathsf{A}}$; morover, it is almost an exact orbit except for the jump from $\mathcal{R}_{\mathsf{A}}^{k'}(h_{\mathsf{A}})$ to $\mathcal{R}_{\mathsf{A}}^{-k''}(h_{\mathsf{B}})$. If k is large enough, then both $\mathcal{R}_{\mathsf{A}}^{k'}(h_{\mathsf{A}})$ and $\mathcal{R}_{\mathsf{A}}^{-k''}(h_{\mathsf{B}})$ are close to f_{A}, so that this jump is small, as shown in Figure 4. We can, therefore, write $\mathcal{R}_{\mathsf{A}^{\star k}}(h_{\mathsf{A}}) = \mathcal{R}_{\mathsf{A}}^{k}(h_{\mathsf{A}}) \approx h_{\mathsf{B}}$.

Similarly, the sequence $\left(h_{\mathsf{B}}, \mathcal{R}_{\mathsf{B}}(h_{\mathsf{B}}), \ldots, \mathcal{R}_{\mathsf{B}}^{m''}(h_{\mathsf{B}}), \mathcal{R}_{\mathsf{B}}^{-m'}(h_{\mathsf{A}}), \ldots, \mathcal{R}_{\mathsf{B}}^{-1}(h_{\mathsf{A}}), h_{\mathsf{A}}\right)$ is a pseudoorbit of $\mathcal{R}_{\mathsf{B}}$, which is an exact orbit everywhere except at the jump from $\mathcal{R}_{\mathsf{B}}^{m''}(h_{\mathsf{B}})$ to $\mathcal{R}_{\mathsf{B}}^{-m'}(h_{\mathsf{A}})$. The larger m, the smaller this jump is because then both $\mathcal{R}_{\mathsf{B}}^{m''}(h_{\mathsf{B}})$ and $\mathcal{R}_{\mathsf{B}}^{-m'}(h_{\mathsf{A}})$ are close to f_{B} (see Figure 4), hence we can write $\mathcal{R}_{\mathsf{B}^{\star m}}(h_{\mathsf{B}}) = \mathcal{R}_{\mathsf{B}}^{m}(h_{\mathsf{B}}) \approx h_{\mathsf{A}}$.

We have, thus, constructed an approximate fixed point of the composition $\mathcal{R}_{\mathsf{A}^{\star k}} \circ \mathcal{R}_{\mathsf{B}^{\star m}}$:

$$\mathcal{R}_{\mathsf{A}^{\star k}} \circ \mathcal{R}_{\mathsf{B}^{\star m}}(h_{\mathsf{B}}) \approx h_{\mathsf{B}} \ .$$

The sequence $\widetilde{\mathcal{O}}_{(\mathsf{A}^{\star k}, \mathsf{B}^{\star m})^{\star \infty}}$ can be thought of as a pseudoorbit of the operator $\mathcal{R}$ (23) that is periodic with period $k+m$.

Using the assumptions of hyperbolicity of the fixed points f_{A} and f_{B} and transversality of the intersection of the unstable manifold of each of these fixed points with the stable manifold of the other one, we prove in [35] the existence of a fixed point of the renormalization operator $\mathcal{R}_{\mathsf{A}^{\star k} \star \mathsf{B}^{\star m}}$ corresponding to the composition $\mathsf{A}^{\star k} \star \mathsf{B}^{\star m}$. The proof is based on constructing a true periodic orbit $\mathcal{O}_{(\mathsf{A}^{\star k}, \mathsf{B}^{\star m})^{\star \infty}}$ of period $k+m$ of $\mathcal{R}$ (23), which is shadowed by the pseudo-orbit $\widetilde{\mathcal{O}}_{(\mathsf{A}^{\star k}, \mathsf{B}^{\star m})^{\star \infty}}$. The points of the periodic orbit $\mathcal{O}_{(\mathsf{A}^{\star k}, \mathsf{B}^{\star m})^{\star \infty}}$ are represented by the symbol + in Figure 4. This orbit is used, in turn, to construct the fixed point $f_{\mathsf{A}^{\star k} \star \mathsf{B}^{\star m}}$ of the operator of $\mathcal{R}_{\mathsf{A}^{\star k} \star \mathsf{B}^{\star m}}$.

The scaling exponent $\delta_{\mathsf{A}^{\star k} \star \mathsf{B}^{\star m}}$ is equal to the unstable eigenvalue of the linearization of $\mathcal{R}_{\mathsf{A}^{\star k} \star \mathsf{B}^{\star m}}$ around its fixed point $f_{\mathsf{A}^{\star k} \star \mathsf{B}^{\star m}}$. In turn, the fixed point $f_{\mathsf{A}^{\star k} \star \mathsf{B}^{\star m}}$ is constructed from the pseudoorbit $\widetilde{\mathcal{O}}_{\mathsf{A}^{\star k}, \mathsf{B}^{\star m}}$. If we denote the $k+m$ points of $\widetilde{\mathcal{O}}_{\mathsf{A}^{\star k}, \mathsf{B}^{\star m}}$ by Z_1, Z_2, ..., Z_{k+m}, then this implies that

$$D\mathcal{R}_{\mathsf{A}^{\star k} \star \mathsf{B}^{\star m}}(f_{\mathsf{A}^{\star k} \star \mathsf{B}^{\star m}}) \approx \prod_{j=1}^{k+m} D\mathcal{R}(Z_j) \ .$$

From the dynamics of $\mathcal{R}$ it is intuitively clear that most of the points Z_j are close to f_{A} or to f_{B} (a precise quantitative statement is the main part of [35]). If k increases, then the new points added to the pseudoorbit $\widetilde{\mathcal{O}}_{\mathsf{A}^{\star k}, \mathsf{B}^{\star m}}$ will be close to f_{A}, while if m increases, the new points will be close to f_{B}. For a point Z_j in a neighborhood of f_{A}, $D\mathcal{R}(Z_j) \approx D\mathcal{R}_{\mathsf{A}}(f_{\mathsf{A}}) = \delta_{\mathsf{A}}$, and, similarly, for Z_j in a neighborhood of f_{B}, $D\mathcal{R}(Z_j) \approx D\mathcal{R}_{\mathsf{B}}(f_{\mathsf{B}}) = \delta_{\mathsf{B}}$. This implies that

$$\delta_{\mathsf{A}^{\star k+1} \star \mathsf{B}^{\star m}} = D\mathcal{R}_{\mathsf{A}^{\star k+1} \star \mathsf{B}^{\star m}}(f_{\mathsf{A}^{\star k+1} \star \mathsf{B}^{\star m}}) \approx \delta_{\mathsf{A}^{\star k} \star \mathsf{B}^{\star m}} \, \delta_{\mathsf{A}} \ .$$

This reasoning gives some intuitive explanation of the fact that the ratio of the parameter-space scaling exponents, $\frac{\delta_{\mathsf{A}^k \mathsf{B}}}{(\delta_{\mathsf{A}})^k \delta_{\mathsf{B}}}$, tends to a limit as k tends to ∞ (see part (ii) of PACSE). The other parts of PACSE can also be explained within this construction. We refer the reader to our paper [35] for more details.

Acknowledgements AO thanks Ana Pérez for her computational support. We would like to thank Hans Koch and Lluís Alsedà for interesting discussions.

References

1. The GMP home page. URL www.swox.com/gmp/
2. Apte, A., Wurm, A., Morrison, P.J.: Renormalization and destruction of $1/\gamma^2$ tori in the standard notwist map. Chaos **13**(2), 421–433 (2003)
3. Arnol'd, V.I.: Small denominators. I. Mapping the circle onto itself. Izv. Akad. Nauk SSSR Ser. Mat. **25**, 21–86 (1961). Correction: 28:479–480, 1964; English translation: *Amer. Math. Soc. Transl. (2)*, 46:213–284, 1965
4. Brent, R.P.: Algorithms for Minimization Without Derivatives. Prentice-Hall, Englewood Cliffs, N.J. (1973)
5. Briggs, K.M.: The doubledouble homepage. URL www.labs.bt.com/people/briggsk2/doubledouble.html
6. del Castillo-Negrete, D., Greene, J.M., Morrison, P.J.: Renormalization and transition to chaos in area preserving nontwist maps. Phys. D **100**(3-4), 311–329 (1997)
7. Chang, S.J., McCown, J.: Universal exponents and fractal dimensions of Feigenbaum attractors. Phys. Rev. A (3) **30**(2), 1149–1151 (1984)

8. Christiansen, F., Cvitanović, P., Rugh, H.H.: The spectrum of the period-doubling operator in terms of cycles. J. Phys. A **23**(14), L713–L717 (1990). This article also appears in J. Phys. A **23**(22), L7135–L7175 (1990)
9. Collet, P., Eckmann, J.P.: Iterated Maps on the Interval as Dynamical Systems. Birkhäuser, Boston (1980)
10. Collet, P., Eckmann, J.P., Koch, H.: On universality for area-preserving maps of the plane. Phys. D **3**(3), 457–467 (1981)
11. Collet, P., Eckmann, J.P., Koch, H.: Period doubling bifurcations for families of maps on $\mathbf{R}^n$. J. Statist. Phys. **25**(1), 1–14 (1981)
12. Cvitanović, P., Gunaratne, G.H., Vinson, M.J.: On the mode-locking universality for critical circle maps. Nonlinearity **3**(3), 873–885 (1990)
13. De Carvalho, A., Lyubich, M., Martens, M.: Renormalization in the Hénon family. I. Universality but non-rigidity. J. Stat. Phys. **121**(5-6), 611–669 (2005)
14. Derrida, B., Gervois, A., Pomeau, Y.: Iteration of endomorphisms on the real axis and representation of numbers. Ann. Inst. H. Poincaré Sect. A (N.S.) **29**(3), 305–356 (1978)
15. Derrida, B., Gervois, A., Pomeau, Y.: Universal metric properties of bifurcations of endomorphisms. J. Phys. A **12**(3), 269–296 (1979)
16. Eckmann, J.P., Koch, H., Wittwer, P.: A computer-assisted proof of universality for area-preserving maps. Mem. Amer. Math. Soc. **47**(289), vi+122 (1984)
17. Eckmann, J.P., Wittwer, P.: A complete proof of the Feigenbaum conjectures. J. Statist. Phys. **46**(3-4), 455–475 (1987)
18. Feigenbaum, M.J.: Quantitative universality for a class of nonlinear transformations. J. Statist. Phys. **19**(1), 25–52 (1978)
19. Feigenbaum, M.J.: The universal metric properties of nonlinear transformations. J. Statist. Phys. **21**(6), 669–706 (1979)
20. Feigenbaum, M.J., Kadanoff, L.P., Shenker, S.J.: Quasiperiodicity in dissipative systems: a renormalization group analysis. Phys. D **5**(2-3), 370–386 (1982)
21. Finch, S.R.: Mathematical Constants. Cambridge University Press, Cambridge (2003)
22. Forsythe, G.E., Malcolm, M.A., Moler, C.B.: Computer Methods for Mathematical Computations. Prentice-Hall, Englewood Cliffs, N.J. (1977)
23. Gaidashev, D., Koch, H.: Renormalization and shearless invariant tori: numerical results. Nonlinearity **17**(5), 1713–1722 (2004)
24. Gaidashev, D., Yampolsky, M.: Cylinder renormalization of Siegel disks. Experiment. Math. **16**(2), 215–226 (2007)
25. Gaidashev, D.G.: Cylinder renormalization for siegel discs and a constructive measurable Riemann mapping theorem. Nonlinearity **20**(3), 713–741 (2007)
26. Ge, Y., Rusjan, E., Zweifel, P.: Renormalization of binary trees derived from one-dimensional unimodal maps. J. Statist. Phys. **59**(5-6), 1265–1295 (1990)
27. Graczyk, J., Świątek, G.: Siegel disks with critical points in their boundaries. Duke Math. J. **119**(1), 189–196 (2003)
28. Hardy, G.H., Wright, E.M.: An Introduction to the Theory of Numbers. Oxford (1990)
29. Herman, M.R.: Sur la conjugaison différentiable des difféomorphismes du cercle à des rotations. Inst. Hautes Études Sci. Publ. Math. (49), 5–233 (1979)
30. Katok, A., Hasselblatt, B.: Introduction to the Modern Theory of Dynamical Systems. Cambridge University Press, Cambridge (1995)
31. Katznelson, Y., Ornstein, D.: The differentiability of the conjugation of certain diffeomorphisms of the circle. Ergodic Theory Dynamical Systems **9**(4), 643–680 (1989)
32. Ketoja, J.A., Kurkijärvi, J.: Binary tree approach to scaling in unimodal maps. J. Statist. Phys. **75**(3-4), 643–668 (1994)
33. Khanin, K., Teplinsky, A.: Herman's theory revisited. Invent. Math. **178**(2), 333–344 (2009)
34. de la Llave, R., Olvera, A.: The obstruction criterion for non-existence of invariant circles and renormalization. Nonlinearity **19**(8), 1907–1937 (2006)
35. de la Llave, R., Olvera, A., Petrov, N.P.: A shadowing theorem for heteroclinic cycles with applications to properties of scaling exponents. Preprint (2010)
36. de la Llave, R., Olvera, A., Petrov, N.P.: Universal scalings of universal scaling exponents. J. Phys. A **40**(22), F427–F434 (2007)
37. de la Llave, R., Petrov, N.P.: Regularity of conjugacies between critical circle maps: an experimental study. Experiment. Math. **11**(2), 59–81 (2002)
38. de la Llave, R., Petrov, N.P.: Boundaries of Siegel disks – numerical studies of their dynamics and regularity. Chaos **18**(3), 962–987 (2008)
39. Luque, A., Villanueva, J.: Computation of derivatives of the rotation number for parametric families of circle diffeomorphisms. Phys. D **237**(20), 2599–2615 (2008)
40. MacKay, R.S.: A renormalisation approach to invariant circles in area-preserving maps. Phys. D **7**(1-3), 283–300 (1983)
41. MacKay, R.S.: Renormalisation in Area-Preserving Maps. World Scientific, River Edge, NJ (1993)
42. Manton, N.S., Nauenberg, M.: Universal scaling behaviour for iterated maps in the complex plane. Comm. Math. Phys. **89**(4), 555–570 (1983)
43. Mather, J.N.: Nonexistence of invariant circles. Ergodic Theory Dynam. Systems **4**(2), 301–309 (1984)
44. de Melo, W., van Strien, S.: One-Dimensional Dynamics. Springer-Verlag, Berlin (1993)
45. Moser, J.: A rapidly convergent iteration method and non-linear differential equations. II. Ann. Scuola Norm. Sup. Pisa (3) **20**, 499–535 (1966)
46. Olvera, A.: Contribucion al estudio de la aplicacion standard. Ph.D. thesis, UNAM (1988)

47. Olvera, A., Petrov, N.P.: Regularity properties of critical invariant circles of twist maps, and their universality. SIAM J. Appl. Dyn. Systems **7**(3), 962–987 (2008)
48. Olvera, A., Simó, C.: The obstruction method and some numerical experiments related to the standard map. In: Periodic solutions of Hamiltonian systems and related topics (Il Ciocco, 1986), pp. 235–244. Reidel, Dordrecht (1987)
49. Olvera, A., Simó, C.: An obstruction method for the destruction of invariant curves. Phys. D **26**(1-3), 181–192 (1987)
50. Ostlund, S., Rand, D., Sethna, J., Siggia, E.D.: Universal properties of the transition from quasiperiodicity to chaos in dissipative systems. Phys. D **8**(3), 303–342 (1983)
51. Shenker, S.J.: Scaling behavior in a map of a circle onto itself: empirical results. Phys. D **5**(2–3), 405–411 (1982)
52. Shenker, S.J., Kadanoff, L.P.: Critical behavior of a KAM surface. I. Empirical results. J. Statist. Phys. **27**(4), 631–656 (1982)
53. Siegel, C.L.: Iteration of analytic functions. Ann. of Math. (2) **43**, 607–612 (1942)
54. Sinai, Y.G., Khanin, K.M.: Smoothness of conjugacies of diffeomorphisms of the circle with rotations. Uspekhi Mat. Nauk **44**(1(265)), 57–82, 247 (1989). English translation: Russian Math. Surveys, **44**(1), 69–99 (1989)
55. Singer, D.: Stable orbits and bifurcation of maps of the interval. SIAM J. Appl. Math. **35**(2), 260–267 (1978)
56. de Sousa Vieira, M.C.: Scaling factors associated with M-furcations of the $1 - \mu|x|^z$ map. J. Statist. Phys. **53**(5-6), 1315–1325 (1988)
57. Stark, J.: Smooth conjugacy and renormalisation for diffeomorphisms of the circle. Nonlinearity **1**(4), 541–575 (1988)
58. Stirnemann, A.: Renormalization for golden circles. Comm. Math. Phys. **152**(2), 369–431 (1993)
59. Stirnemann, A.: Existence of the Siegel disc renormalization fixed point. Nonlinearity **7**(3), 959–974 (1994)
60. Stirnemann, A.: A renormalization proof of Siegel's theorem. Nonlinearity **7**(3), 943–958 (1994)
61. Stirnemann, A.: Towards an existence proof of MacKay's fixed point. Comm. Math. Phys. **188**(3), 723–735 (1997)
62. Tresser, C., Coullet, P.: Itérations d'endomorphismes et groupe de renormalisation. C. R. Acad. Sci. Paris Sér. A-B **287**(7), A577–A580 (1978)
63. Vilela Mendes, R.: Critical point dependence of universality in maps of the interval. Phys. Lett. A **84**(1), 1–3 (1981)
64. Widom, M.: Renormalization group analysis of quasiperiodicity in analytic maps. Comm. Math. Phys. **92**(1), 121–136 (1983)
65. Wilson, K.G.: Renormalization group and critical phenomena. I. Renormalization group and the Kadanoff scaling picture. Phys. Rev. B **4**(9), 3174–3183 (1971)
66. Yoccoz, J.C.: Conjugaison différentiable des difféomorphismes du cercle dont le nombre de rotation vérifie une condition diophantienne. Ann. Sci. École Norm. Sup. (4) **17**(3), 333–359 (1984)
67. Yoccoz, J.C.: Il n'y a pas de contre-exemple de Denjoy analytique. C. R. Acad. Sci. Paris Sér. I Math. **298**(7), 141–144 (1984)
68. Yoccoz, J.C.: Analytic linearization of circle diffeomorphisms. In: Dynamical Systems and Small Divisors (Cetraro, 1998), *Lecture Notes in Math.*, vol. 1784, pp. 125–173. Springer, Berlin (2002)